Distributed Magnetic Self-Assembly Inspired by Protein Folding

Emily Jayne Southern

MSc by Research

University of York
Electronic Engineering

December 2017

Abstract

The goal of artificial self-assembly has been pursued for many decades in order to improve manufacturing at small scales and also to understand more about the process of self-assembly in nature. However, many previous approaches to this problem are limited either in their ability to be used at small scales or in their ability to produce complex, heterogeneous structures. In this thesis, preliminary work has been carried out on an approach that uses tiles and permanent magnets which can reconfigure from a 1D chain to a 2D shape. Inspiration for the system was drawn from the enthalpic self-assembly of protein chains into their native states. As such, the magnet paths are designed such that, after initiation, the magnets reconfigure and change the chain geometry into the shape desired by the user. The final structure is pre-determined while the actuation occurs in an entirely bottom-up matter. The system uses no electronic components and is likely to scale down in size favourably. Inequalities that constrain the internal geometry of the tiles are derived, and the system is shown to work successfully in both simulation and physical experiments. Finally, simulations containing large numbers of tiles are presented to indicate the capability of the system to produce detailed and potentially functional structures.

Contents

List of Tables

List of Figures

Accompanying Material

The supplementary video accompanying this thesis, showing footage from experiments, can be found at the University of York White Rose eTheses Repository. A hard copy (CD) of the supplementary video can be found at the back of this thesis.

Acknowledgements

I wish to thank the following people for their help and support during the writing of this thesis:

- My supervisor, Dr. Shuhei Miyashita
- All members of the Micro-Robotics lab during my time at the University of York: Valentin Besnard, Julien Delmas, Yoshitaka Iwata, Haruna Iwasaki, Etienne Perroux, Sam Perry, and Alexis Du Plessis D'Argentre
- All members of the Department of Electronic Engineering, both students and faculty, with whom I have discussed my work
- My family and friends.

Declaration of Authorship

I, EMILY JAYNE SOUTHERN, declare that this thesis titled, 'DISTRIBUTED MAGNETIC SELF-ASSEMBLY INSPIRED BY PROTEIN FOLDING' and the work presented in it are my own. I confirm that:

- This work was done wholly or mainly while in candidature for a research degree at this University.
- Where any part of this dissertation has previously been submitted for a degree or any other qualification at this University or any other institution, this has been clearly stated.
- Where I have consulted the published work of others, this is always clearly attributed.
- Where I have quoted from the work of others, the source is always given. With the exception of such quotations, this thesis is entirely my own work.
- I have acknowledged all main sources of help.
- Where the thesis is based on work done by myself jointly with others, I have made clear exactly what was done by others and what I have contributed myself.

Chapter 1

Background and Motivation

Regarding the origins of life on Earth, one of the key questions that remains is how individual microbes came to work together and produce larger, more complex structures. The 'primordial soup' theory, first stated by Alexander Oparin in 1924 [17], claims that the simple compounds that existed during the formation of Earth were able to combine together into more complex compounds by using the free energy available in their environment. A remarkable aspect of this phenomenon is that, barring the idea of some 'God'-like presence overseeing the soup, all of the information and physical capabilities required to construct these increasingly intricate compounds already existed within the microbes. Thus, it could be regarded as the original example of self-directed assembly, whereby a system of parts assembles in a 'bottom-up' manner into a more complex structure without requiring any external interference.

Although self-directed assembly is believed to be the original method of construction used in nature, mankind has, for the majority of its existence, depended on a 'top-down' approach of assembly; that is, a human (or a machine built by a human) is the external provider of intelligence and physical manoeuvrability that assembles a collection of parts into a more complex whole. This has been advantageous to the human race for millennia as we are able to directly enforce our vision onto materials without having to create an environment that would naturally self-assemble the outcome that we want. Nevertheless, the idea of a desired item taking shape independently of human oversight is a pleasing one, as the amount of physical input into the creation of objects would be drastically reduced. Furthermore, if, in the future, we were able to create a method in which a set of initial conditions can produce any type of item that we desire, not only would this be extremely advantageous in terms of manufacturing, but we may also be able to discover more about how primitive organisms came to be in the first place.

Research on this project was carried out from approximately September 2016 to August 2017.

The thesis is structured as follows:

- Chapters 2 and 3 cover results from the literature and a list of design specifications for the project is derived
- Chapter 4 covers development of the project's first design iteration
- Chapter 5 discusses the issue of collision in chain-type systems and draws conclusions about the level of universality the system possesses
- Chapter 6 contains development of the project's second design iteration and the theoretical contributions made by the project
- Chapters 7 and 8 present results both in simulation and in physical experiments, as well as concluding remarks and discussion of future work

Chapter 2

Literature Review

2.1 Introduction

Self-assembly is a topic spanning various fields such as biology, chemistry, materials science and engineering. Broadly speaking, it is the process of individual parts coming together with no external direction to form an organised structure.

As the areas of research based on the concept of self-assembly are so diversely located, it is all the more important to be aware of the main strands of research and how they are linked together. By the end of this chapter it will be clear that it is difficult to determine if any of the results from each area are definitively better than any other.

The structure of this review is as follows: Firstly, the definition of 'self-assembly' is discussed, and the rules for which papers are considered within scope and out of scope for this work are determined. Next, past literature is scrutinised based on the main method of approach used: mechanical, chemical, magnetic, DNA-based, and enthalpic. Key papers from each of these areas will be described in more detail. A table summarising the general benefits and drawbacks of each approach is presented at the end of this section. Finally, the summary will identify key gaps in the literature that must be filled in order for the field as a whole to progress.

2.1.1 Self-Assembly

In the past, the words 'self-assembly' and 'self-organisation' have been used interchangeably or with varying definitions depending on the field of research in which they have been used. Uskokovic [18] goes so far as to say that both of these words are used incorrectly, since it is impossible to separate the topics of module assembly and the influence

of the modules' environment on assembly, and that both should be replaced by the single term 'co-assembly'. The review by Halley and Winkler [19] states four key differences between the the two:

1. Self-assembling systems can only display simple emergent behaviour while self-organising systems can also display complex emergent behaviour. This is because a self-assembling system does not have access to a constant source of energy, so the system is constantly approaching an energy minimum, and the modules are not irreversibly changed during the actuation process.

2. The modules in a self-assembling system are heterogeneous and it is the local interaction of different modules that produces the collective behaviour, whereas the modules in a self-organising system are typically homogeneous.

3. There is no minimum number of modules required for a self-assembling system - two modules bonding together could be considered an example of self-assembly. A larger (but as yet not clearly defined) number of modules are required in order for self-organising behaviour to be exhibited.

4. A self-assembling system has a final state at which no more modules can be added, while the number of modules in a self-organising could, in theory, be increased indefinitely.

The term 'self-assembly' can itself be split into sub-types in accordance with the proposal by Whitesides and Grzybowski [20]. These are:

1. Static self-assembly- dissipates energy.

2. Dynamic self-assembly- does not dissipate energy.

3. Templated self-assembly- the environment containing the modules dictates the shape of the final structure.

4. Biological self-assembly- a combination of (1) and (2) that brings about complex biological processes.

Comparing the two lists above, static self-assembly in the second list can be equated to self-assembly in the first list, and dynamic self-assembly in the second list could be equated to self-organisation in the first list. From here on, the definitions of 'self-assembly' and 'self-organisation' will correlate to those in the first list, while being cognisant that they could also be referred to as static and dynamic self-assembly, respectively.

Although the output of this dissertation would be considered an example of self-assembling behaviour, literature concerning work on self-organising behaviour will also be included. Nonetheless, some lines must be drawn as to what should be excluded from this work. A useful litmus test to decide this is to use the concept of *emergence* [21] [22]: when smaller modules are aggregated to produce a larger structure, they are able to display abilities that they would otherwise not be able to display on their own. Similarly, for this work, most attention is paid to previous research in which the individual modules do not possess the abilities of the final assembly that they create. In this way, the line between self-assembling/self-organising systems and closely related fields such as swarm robotics, modular robotics, and micro-machining, can be clearly demarcated.

2.2 Key Areas of Self-Assembly Research

For ease of reading, the literature has been categorised based on the type of technique utilised in each work. It is natural that some of the works presented could be placed in more than one category; in these cases, the work is categorised based on what is believed to be the primary technique used.

2.2.1 Mechanical Self-Assembly

The first notable work on mechanical self-assembling systems was that of Lionel Penrose in his seminal 1959 paper 'Self-Reproducing Machines' [1]. The modules presented in this paper are made entirely of plywood and are agitated in a container in order to supply them with kinetic energy. The modules cannot connect together until an initial 'seed' composed of two already connected modules is added to the container. Due to the change in resting angle of the connected modules and the modules' geometry, free modules that interact with the seed change angle and connect to the seed (see Figure 2.1). Later, more complicated modules contain extra features so that the aggregate of connected modules splits in two once a certain number of modules have been added. By demonstrating that seemingly intelligent behaviour such as self-assembly and self-replication could be carried out purely mechanically, Penrose introduced the concept of intelligence being embedded in a physical structure rather than it requiring a control centre such as a brain. This idea is now being used to analyse how simple organisms were able to develop into complex structures, and also in the construction of robots following the paradigm now generally known as *morphological computation* [23].

Altering the addressability of each module is a method often used in self-assembling systems. Here, addressibility is defined as 'where every component is distinct and is

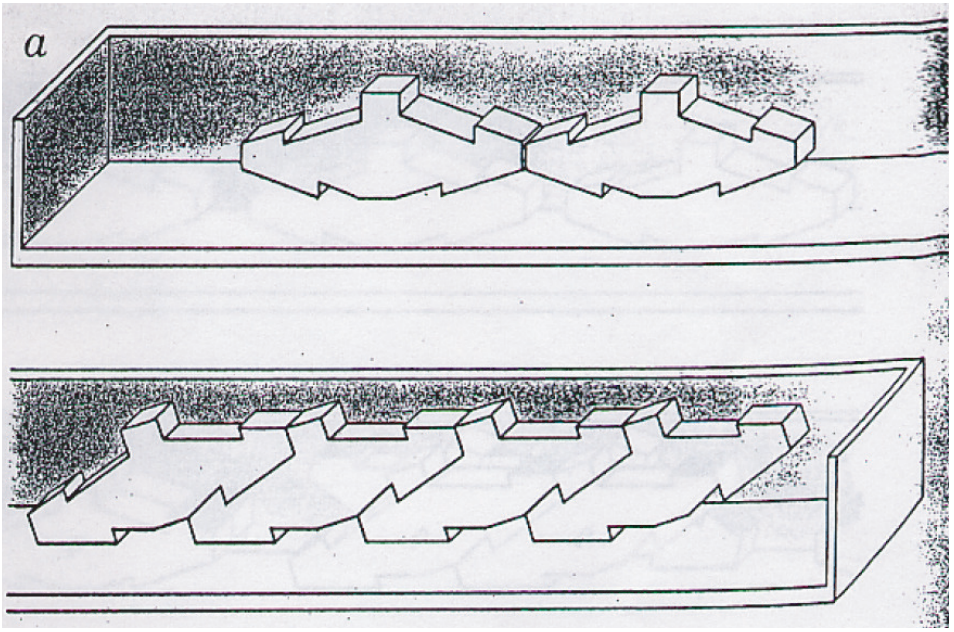

FIGURE 2.1: One type of Penrose's units. Reproduced from [1].

programmed to occupy a specific location within a target structure' [24] - by making some modules physically incapable of bonding in certain spatial or temporal situations, structures with a higher order of complexity can be produced. Masumori and Tanaka [25] develop convex and concave patterns for the edges of their cubic modules that, when agitated with a shaker, configure into predetermined letters of the alphabet. Boncheva et al. [26] use patterned solder dots on the edges of their triangular prism-shaped modules to achieve addressability in a system that is also able to work as an electronic device. The system is shaken and heated to melt the solder dots, which are then attracted to each other through capillary interactions. The patterning of dots on each force is designed such that every dot on each colliding face need to align in order for the modules to bond. The LEDs in the resulting structure can then be illuminated by connecting one of the modules to a power source. Similarly, Matsumoto and Hashimoto [27] use both solder and hot-melt adhesive in order to assemble modules in two distinct stages, in response to the temperature of the environment. A mortise-and-tenon connection for the modules is also proposed to increase the addressability of the system, as it forces modules to connect only at pre-specified orientations.

Another notable investigation into the effects of a module's shape in self-assembly is that presented by Virgo et al. in 'Evolvable Physical Self-Replicators' [2]. The modules in this paper were carefully designed such that, if the modules collide at an unfavourable angle, they can pivot around each other and lock into a more stable configuration. Although the modules were made at the mesoscale level (each module being several centimetres in length), the aim was to unearth the types of issues that would be found

if the system were to be reproduced on the molecular level. They defined these issues as: product inhibition, cyclization, spontaneous ligation, and elongation at staggered ends (see Figure 2.2). The conclusions from this paper, namely that the development of a module able to circumvent all these issues is a very complex process, give rise to the suspicion that it would not be possible for a molecule with all of these attributes to be produced through natural selection. Thus it could be surmised that in biological systems it is complex interactions between simple modules, rather than simple interactions with complex structures, that produces intelligent assembly.

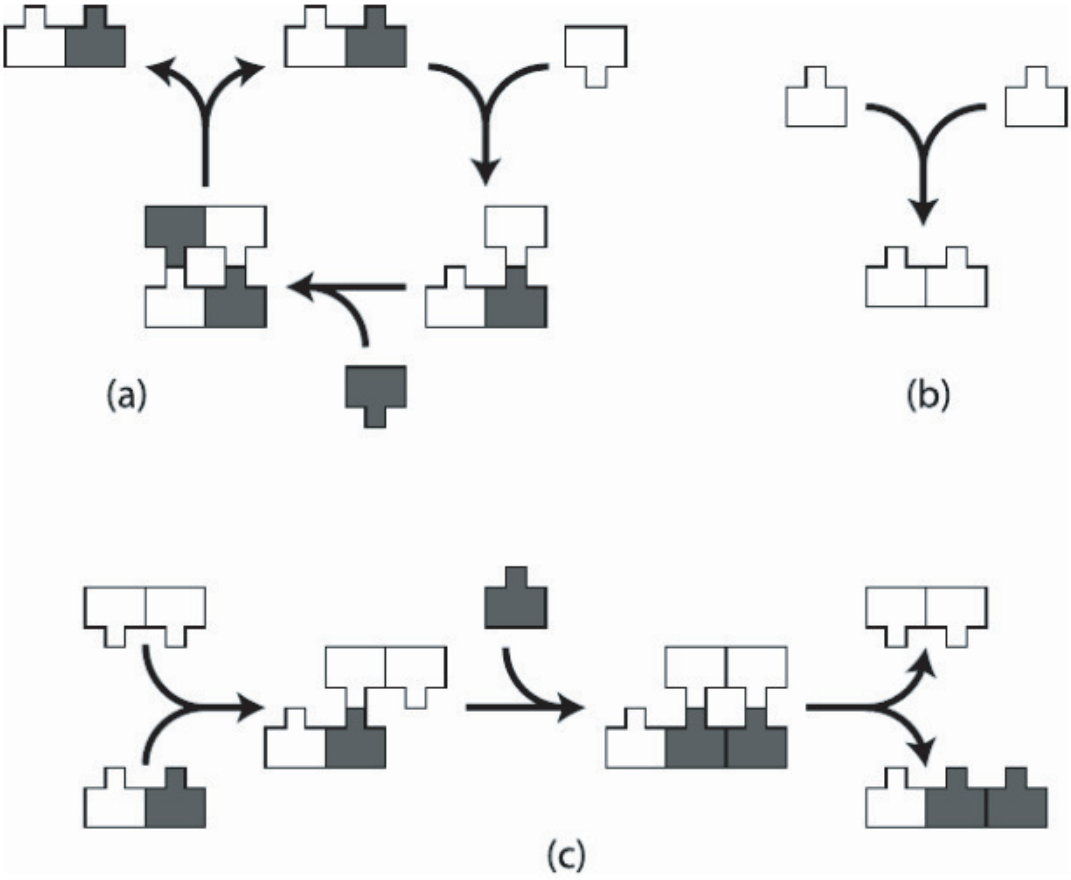

FIGURE 2.2: Examples of issues that arise in self-assembly. (a) Correct self-assembly. (b) Two modules assemble incorrectly, an example of spontaneous ligation. (c) Modules that have assembled through spontaneous ligation cause an incorrect sequence, an example of the elongation catastrophe. Reproduced from [2].

The works presented so far have used dynamic environments (a container that is agitated in [1], [25] and [26], and a modified air hockey table in [2]) to provide their systems with kinetic energy and to add an element of stochasticity to the environment, as all of them rely on the existence of random interactions between modules in order for the modules to bind together. However, there are alternative methods which can provide modules with energy in a more deterministic manner. In [28], Mitsui et al. use what they define as a 'self-assembly printer' to rotate and output modules in the correct order as defined

by the user. Copper foil on the faces of the modules allow the printed assembly to produce an LED display. Meanwhile, Vergara et al. [29] develop modules composed of a hard cube encased in a pneumatically actuated shell. By inflating specific modules in an assembly, various mechanisms such as locomotion and self-reconfiguration can be successfully demonstrated. However, as each module requires its own micro air pump in order to be inflated, significant developments in fabrication methods will be required in order for the system to be considered scalable. Considerable exploration has been made into planning algorithms for self-assembly with modules that can communicate wirelessly [30] [31] [32] [33] with the assumption that each module can move about independently. Analysis of these algorithms is beyond the scope of this work; however, a review of the current state of the field can be found here [34]. A publication series worthy of specific attention concerns the Modular Transformer, or 'M-TRAN' [35]. The creators combined features of both lattice- and chain-type systems to produce a robot capable of various forms of locomotion, as well as the ability to navigate through or over difficult terrain. A camera system and LED transmitters were used for docking extra modules in order to increase robot size [36].

Another series of papers on mechanical self-assembly to be noted in particular is that created by the DARPA Programmable Matter program commissioned in 2006. The original proposal was for the creation of a 'smart dust', and the program statement concludes by stating that

> manufacturing of programmable matter devices, while posing a number of significant technical challenges in integration, power, heat management, etc., can be made feasible, and in a relatively short (less than 10 year) time frame with appropriate investment [37] [38].

As this ten-year time frame has already passed and there is still no 'smart dust' in existence, it could be said that the project was a failure. However, the funding for this programme produced various advances in mechanical self-assembly.

Firstly, Cheung et al. [15] produced a system named 'Moteins' which they claim to be 'universally foldable'. In contrast to the research presented thus far, Motein modules are permanently connected in a chain that folds to produce its final 3D structure. Thus, it could be regarded as a $1D \rightarrow 3D$ system as opposed to the $2D \rightarrow 3D$ systems typically shown in other research on foldable robots. As described further in more detail in Chapter 5, the system is able to fold into any desired final shape by converting the graph of the desired shape into one containing a Hamiltonian path. Folding then occurs in a sequence pre-specified by the user until the final shape is produced. Two physical systems were produced for the paper: one of roughly cubic centimetre-size and

one of roughly cubic decimetre-size. Ten modules were produced for the former and eight for the latter, and all were actuated by servo motors within each module. They also produced a physical simulation package that could demonstrate the folding of a 160-module chain into the shape of a wrench.

Next, Gilpin at al. [39] tackled the issue of self-assembling a complex shape by focusing on dis-assembly rather than assembly: $12mm$ cube-shaped blocks were arranged into an array that was larger than the desired $2D$ shape and connected together using electro-permanent magnets. An algorithm determined which modules were unnecessary for the design and magnets on any of these modules would be turned off. The released blocks fall away due to gravity once the final structure is lifted out of the environment. This approach appears more practical than others in terms of complexity, since a reductive manufacturing process such as this would generally be considered simpler than an additive manufacturing process as seen in other systems. However, there were still many issues that were not dealt with in the project, such as scaling the system to three dimensions and reducing the reliance on hardware that cannot reasonably be decreased in size in order for smaller modules to be produced.

The final work to be presented issuing from the DARPA Programmable Matter project is that by Karagozler et al. in 2009 [3]. The main aim for this work was to produce a relatively small module that could also be easily fabricated. The modules (named 'Catoms') were fabricated using a photolithography process that allowed the inclusion of aluminium circuits within the material. The rectangular shapes folded into cylinders after being released from their moulds due to tension in the composite. The outer face of each cylinder was covered with conductive plates in an alternating positive and negative configuration. When two modules were placed next to each other, a series circuit loop was produced between two neighbouring plates on each module. A series of voltages run across the modules to charge and discharge the contacts between them, allowing the modules to roll around each others' surfaces (see Figure 2.3). However, only one module was presented in this paper and it was actuated by placing it on an aluminium sheet connected to electrodes. It is therefore difficult to say whether this experiment was a demonstration of the validity of their theory, or if it was a demonstration of something else entirely. There were also no further hardware-based papers released after this in the series, and so it appears that no further progress has been made so far towards a physical realisation of the system.

The final paper to be presented in this subsection concerns a more theoretical issue in mechanical self-assembly, that of *sequential random bin-picking*. Consider a pair of robotic arms and a bin filled with modules of various types, such that only certain modules can connect to other modules. Every time step, the pair of arms picks two of the

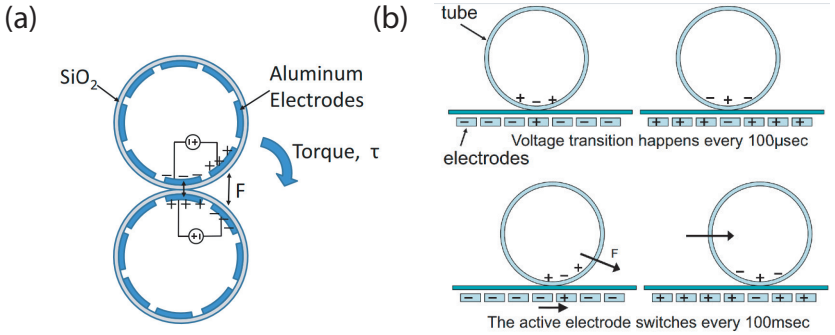

FIGURE 2.3: (a) Illustration of how forces between Catoms are produced between electrodes. (b) Experimental setup of the rolling Catom. The electrodes underneath the tube can be considered an 'unrolled' Catom. Reproduced from [3].

modules at random from the bin and attempts to connect them together: If successful, the connected pair is returned to the bin; if not, both modules are returned to the bin separately. Naturally, there is no order to when specific modules are connected together since they are chosen at random. However, Saitou [40] has developed the concept of a 'conformational change' such that the order can still be chosen even if the bin-picking remains random. The conformational change is a mechanical device within a module such that, when the module is connected to another module, its shape changes so that it allows another module to connect to it.

If there are three modules A, B, C that will eventually form the configuration ABC, they can do so in two orders: $(A + B) + C$ or $A + (B + C)$. Now, a conformational device is added to B such that A and B can only be connected together once B has already connected to a different module, in this case C. The ordering of assembly is now restricted to only $A + (B + C)$. By creating lists of rules defining which modules can connect to which and also when they can connect (before or after a conformational change), vastly precise and complicated structures could in theory be built by a pair of robot arms with minimal intelligence.

2.2.2 Chemical Self-Assembly

We next turn to the works concerning chemical self-assembly. The most prominent advocate of this approach is Professor George Whitesides at Harvard University, whose research in chemical self-assembly is based on the belief that it is the approach most capable of being successful at the meso-scale, where modules are micrometre or millimetre size [4]. Modules above and below this scale may be more well suited to methods of fabrication other than self-assembly, such as fabrication by hand (see Figure 2.4).

Whitesides' specific approach is to coat the edges of modules with a hydrophobic or hydrophilic layer, and then suspend them at the intersection of an aqueous solution and a hydrophobic liquid. The location of the boundary of the two liquids with respect to the modules influences the manner of self-assembly: if the modules float just inside the hydrophobic liquid, then the hydrophobic faces will attract and the hydrophilic faces will repel, and the the reverse will occur if the modules float just inside the aqueous (hydrophilic) solution[41]. This method only allows for two different assembled states for each type of module but, by varying the shapes of the modules and/or the edges of the modules that are coated in each layer, the appearance of these assembled states can vary [42] [43]. Onoe et al. [44] applied an equivalent phenomena between liquids of different pH in their system. Specific faces of the modules were again coated with a hydrophobic or hydrophilic substance but only one solution was used as the environment. When the solution was made weakly acidic the hydrophobic faces were bound together and the modules assembled in pairs. Then, when the solution was made strongly acidic, the hydrophilic faces were bound together and the pairs of modules assembled to form chains. As pH level is not a binary feature like that used in Whitesides' work, it could be possible for more assembly stages to be added to this system and a more complex final structure could be produced.

Instead of altering the environment of the modules, Mao et al. [5] used a series of shape memory polymers (SMPs) with different glass transition temperatures to alter the attributes of the modules in their system. The SMPs are incorporated into a chain such that they will produce a bending moment if actuated. The entire chain is then immersed in a bath of water with a temperature high enough to actuate all seven of the SMPs. The SMPs with a lower actuation temperature will actuate faster than those with a higher actuation temperature, producing a sequential behaviour. This behaviour is necessary to produce certain shapes, such as a spiral (see Figure 2.5).

Finally, Hosokawa et al. [45] used a primarily mechanical system to find analogies between self-assembling systems and chemical reactions. The modules used were homogeneous, triangular units that connected together with permanent magnets when kinetic energy was provided by an apparatus. A 'yield' was said to be produced when six triangles assembled into a hexagon, and each of the five sub-assemblies produced before the hexagon were defined as 'state variables'. Thus, some state variables (such as an assembly of one triangle and an assembly of five triangles) can produce a yield and some (such as an assembly of two triangles and an assembly of five triangles) cannot. It is then possible to calculate the probability of a desired yield being produced through analysing the probabilities of bonding and collision of each module, along with the probability that the correct combinations of sub-assemblies connect together.

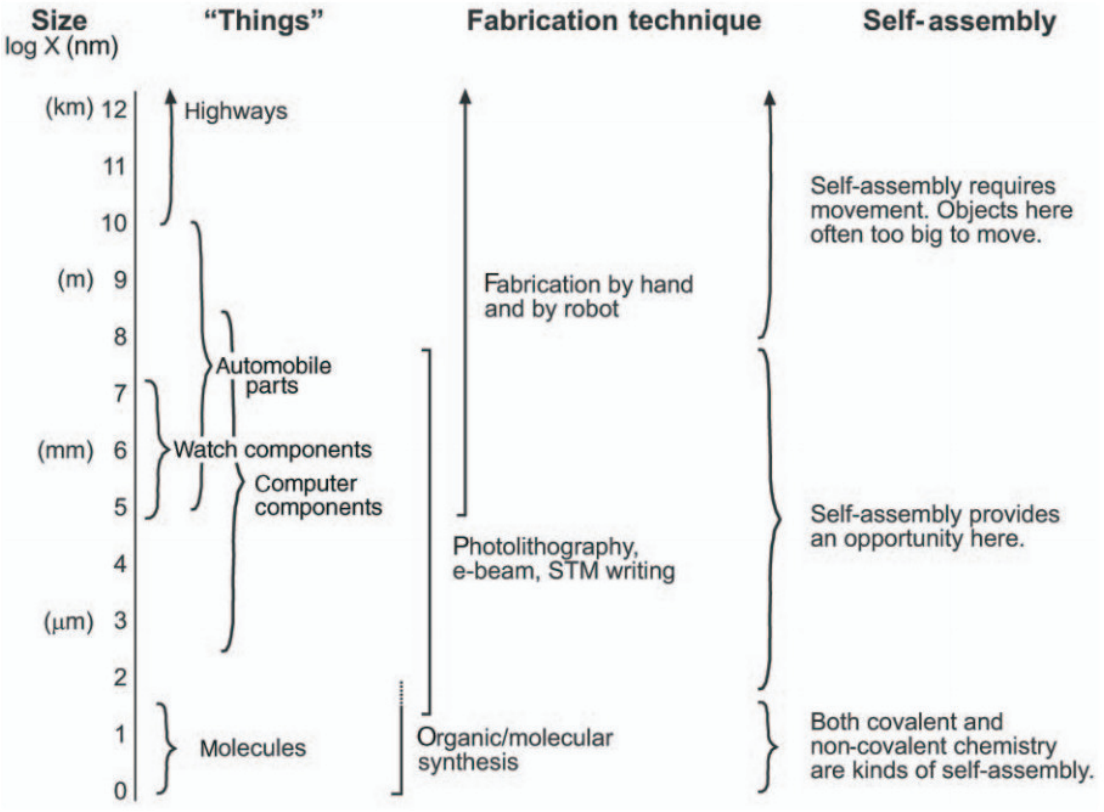

FIGURE 2.4: Chart illustrating the typical fabrication method used at different spatial scales, and the scale at which self-assembly could feasibly be used instead. Reproduced from [4].

2.2.3 Magnetic Self-Assembly

Magnets are often used in self-assembling systems as they can impart kinetic energy to modules without the necessity of bulky and complicated mechanical components. This allows the size of modules to be reduced and the number of modules in an environment to be increased.

Firstly, Ryan et al. [46] and Salehizadeh et al. [47] use a setup of external permanent magnets or electromagnets to control a magnet within an environment. All intelligence regarding the modules is contained within the external setup. The system is able to manipulate spherical magnets with a radius of approximately 250μm, and can move each magnet individually when they are only 750μm apart. Cheang et al. [48] use a similar approach to achieve self-assembly of magnetic microbeads in an environment surrounded by electromagnetic coils. Actuating the coils such that the microbeads rotate at a low frequency causes them to assemble into chains, while a higher frequency causes them to separate. Further, it was noted that a chain of the microbeads has a cone of repulsive magnetic force at both of its ends, meaning that a new bead has to approach from the side of the chain (its 'zone of attraction') in order for it to attach. Chains of up to 13

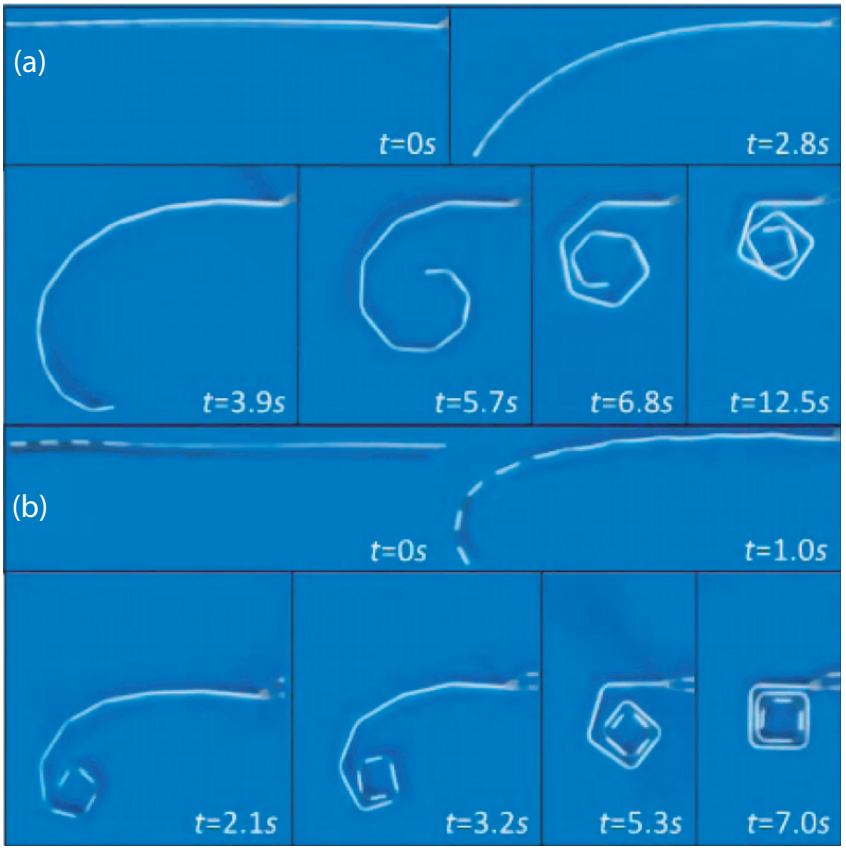

FIGURE 2.5: SMP being folded with (a) uniform hinges that fold simultaneously and (b) with hinges graduated so that they fold sequentially. Reproduced from [5].

beads were produced and some, depending on the number of beads in the chain [49], were able to replicate swimming-like behaviour.

Wang et al. [50] were also capable of producing modules that assemble into chains under the influence of an external magnetic field. However, these modules are floated on an air-water interface and have edges designed like that of a co-sinusoidal curve. This produces an effect similar to [41], [42] and [44] where, through capillary forces, the edges shaped like the peaks and the troughs of the curve attract edges of the same type as its own. The modules assemble randomly when the ratio of peak to trough on the curve was equal but, surprisingly, produce a square-shaped tiling using curves with a $1:2$ ratio. Iwase and Shimoyama [51] use a system of electromagnetic coils to produce a $3D$ assembly in two stages. Initially, a flat design is made comprising the faces and hinges that

will produce the final shape. Two types of hinges are used with different 'sensitivity factors', dependent on the dimensions of the hinge and the volume of ferromagnetic material within the face that the hinge needs to lift. When the strength of the field emanating from the electromagnetic coils is slowly increased, the hinges are actuated and the faces are lifted in the order designated by their sensitivity factor. Interlocking pieces of adjacent faces ensure that the assembled structure remains upright after the assembly has been removed from the field.

Ma et al. [52] were also successful in magnetically transforming a 2D sheet into a 3D structure, using permanent magnets embedded into the structure's faces. Once an initial angular velocity is applied, the magnets in the sheet attract each other and cause a bending moment in the joints built into the sheet, locking into place due to mechanical stops in the structure's design. As such, the simple structure of a cube 'pops' up with only an initial energetic input.

Both Shetye et al. [53] and Masumori et al. [54] apply the technique of including magnets in the areas of the system that need to be reconfigured. The former embeds permanent magnets in silicon components with one pole of the magnet facing out of the component, and patterns a substrate with magnetic regions of the opposite pole. Inserting the substrate into a container filled with components and agitating it causes the components to attach to the magnetic parts of the substrate, while subsequent shaking allows the components to align. The latter, meanwhile, proposes the use of a chain of electromagnets that can produce a folding motion. By relaying the order of polarity for each electromagnet down the chain, it can fold into a shape without the use of motors. The shape can then be held indefinitely by adding a permanent magnet to each face of the modules.

However, the physical experiments presented in the paper did not use electromagnets but only permanent magnets, so it is difficult to say if this approach is as scalable as the authors claim. For example, significant modelling would need to be carried out to ensure that the interference of the electromagnets in close proximity to one another would not impede the actuation of the chain.

Yim and Sitti [6] also demonstrate the ability for magnets to passively configure into a desired shape by encasing large amounts of *mm*-size magnets in silicone rubber. The rubber, cast into the desired final shape of the system, is cut according to an algorithm so that the shape disassembles into a straight chain when tensile stress is applied. The algorithm uses a similar approach to Cheung et al. [15] by finding a Hamiltonian path through each planar layer of the shape, but also includes an algorithm so that the layers of planar Hamiltonian paths can be linked together to form the three-dimensional shape. When the stress is removed, the final shape is recovered through the elastic restoring

forces inherent to the silicone. The magnets provide the additional alignment that allows the chain to stably and precisely restore to its former shape. In contrast to the work by Gilpin et al. [39] which only uses self-disassembly, this work demonstrates the ability of a system to both assemble and disassemble under given conditions.

As the authors encountered difficulties with small chains being difficult to manipulate, a later work [7] introduces the concept of a meta-module: the skeleton of a cube made from the modules presented in the previous paper, reinforced inside its edges with carbon fibre. Both works included demonstrations of 1000-module or meta-module chains that can successfully re-assemble in physical experiments (see Figure 2.6).

The final magnetism-based self-assembly system to be presented here is the work on Soft Cells by Germann et al [8]. The overall concept of Soft Cells is to enclose four permanent magnets in a square configuration inside a cell with a given softness (see Figure 2.7). The cells are linked together in a chain with a central hinge at each join between modules. The entire chain is held taut before being deployed. The permutations of North and South poles in neighbouring cells determine if and in which direction a fold in the chain will occur once the chain is released, while the softness of the cells' material determines the degree of folding. Shapes containing sharp angles and smooth curves could all be produced with the same overall methodology by including modules with varying degrees of stiffness.

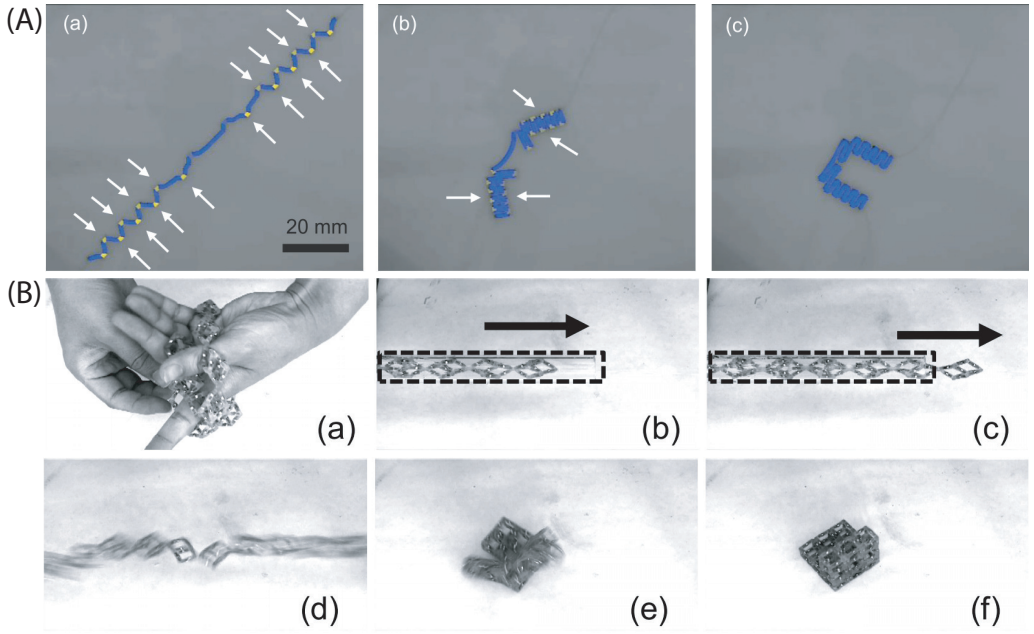

FIGURE 2.6: (A) (a-c) Extension and relaxation of 74 SoftCubes into a C-shape, taken from [6]. (B) (a-f) Extension and relaxation of 9 SoftCube meta-modules into a $9 \times 1 \times 1$ cuboid, reproduced from [7].

2.2.4 DNA-based Self-Assembly

This section briefly introduces the field of DNA self-assembly. This field is growing rapidly and there are hundreds of papers in the area; however, for the sake of brevity and remaining within the scope of this work, only the key paper in this field is presented. The interested reader may wish to look at [55] to gain a wider understanding of this area of research.

The seminal paper on DNA self-assembly is that by Rothemund in 2009 [9], which has been cited over 2500 times at the time of writing. His method, termed 'scaffolded DNA origami', is as follows: the design of the final shape is filled with horizontal cylinders in rows to represent the DNA strand. A 'scaffold' is drawn through the cylinders and they are then linked together at locations which will minimise strain during folding with 'scaffold crossovers', which eventually become 'staples' constructed from DNA base pairs that complement the base pairs of the long DNA strand at that location. These staples cut the long DNA strands at their locations and then rejoin the cut edges to those of the neighbouring cut strands, converting rows of strands into one continuous DNA strand (see Figure 2.8 for a pictorial representation). By combining a long DNA strand, a scaffold material, staples, and small cuts in the strand to facilitate folding, DNA can be folded into geometrically complex shapes at the nano-metre scale.

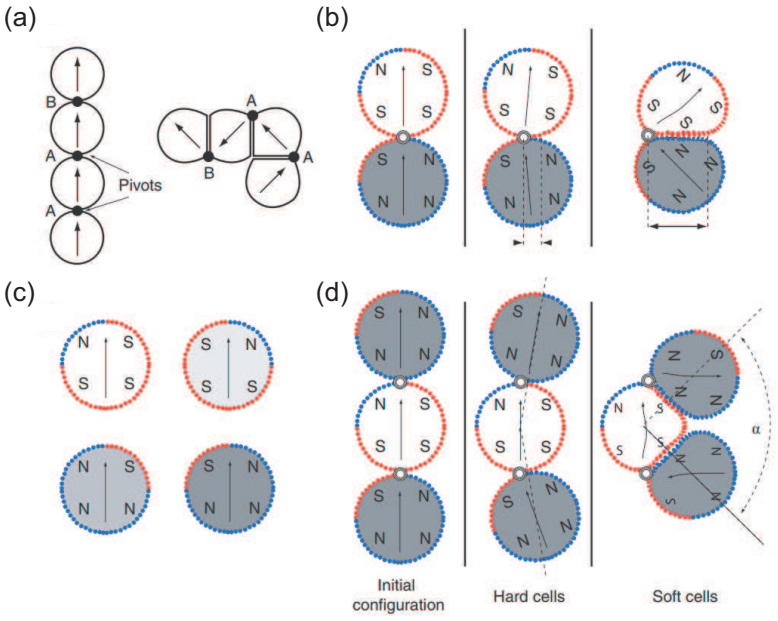

FIGURE 2.7: Concept for the Soft Cells system. (a) Basic principle of the modules and their pivot points. (b) Design of the cells. Blue circles indicate magnets with North pole pointing upwards, red circles indicate magnets with South pole pointing upwards. (c) Folding of two soft cells: initially, final configuration for hard cells, final configuration for soft cells. (d) Folding of three soft cells: Initially, final configuration for hard cells, final configuration for soft cells. Reproduced from [8].

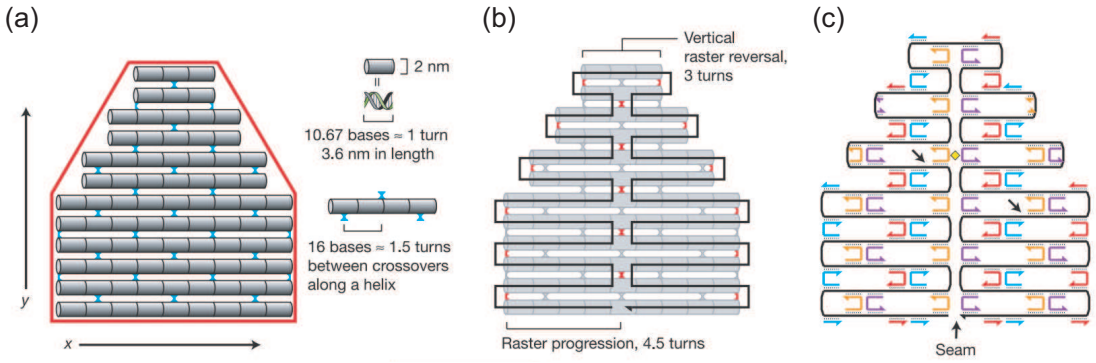

FIGURE 2.8: Design method for scaffolded DNA origami. (a) Desired shape filled with cylinders to represent DNA strands. (b) A scaffold is drawn through the cylinders and scaffold crossovers are marked. (c) Staples composed of the appropriate DNA base pairs are derived and put in position. Reproduced from [9].

2.2.5 Enthalpic Self-Assembly

The final self-assembly approach to be presented here is enthalpic self-assembly. Systems designed with this approach utilise the fact that a closed system, i.e. a system which does not have an external supply of energy, will tend to dissipate energy until it reaches an equilibrium at its lowest energetic state. By carefully designing the modules and the environment in a system such that the desired final shape is at an energetic minimum, one can cause the modules to self-assembly 'naturally'.

Some works in this area achieve self-assembly by altering the topology of energy available in the environment. One of the earliest pieces of research advocating for this method is that by Cohn and Kim in 1991 [56]. Using a known algorithm which provides conditions for ensuring successful crystallisation of a material [57], the authors enable 1000 hexagonal $1mm$-tiles to assemble into an optimally-packed lattice by applying vibrations to the environment. Later, Böhringer et al. [58] use vibration to assemble capacitors and surface-mount diodes into a lattice. They also apply a potential field containing apertures to create a pattern of neutral locations within the environment. Modules added to this environment become 'trapped' in the neutral locations and so the modules assemble to the environment's energetic minimum rather than the modules' energetic minimum. Miyashita et al. [59] use vibrations through water to enable the self-assembly of their modules. The modules vary in shape (circular, square, or square with rounded corners) and in their magnetic properties (containing one or two magnets, with either North or South pole perpendicular to the modules). They discover that varying the shape of the modules considerably alters the time for a lattice to assemble and that an increase in magnetism did not necessarily produce a faster assembly- square-shaped tiles took more time to assemble when they contained two magnets than they did with one.

Another method of manipulating the enthalpy of a system through its environment is by applying microfluidic techniques. Tolley et al. [60] immersed $500\mu m$ tiles in a chamber with eight openings from which the fluid flow through the chamber could be controlled. The chamber also had a patterned base that matched the geometry of the tiles. Varying the fluid flow at the different openings produced a 2D assembly of tiles at a global energetic minimum on the base of the chamber.

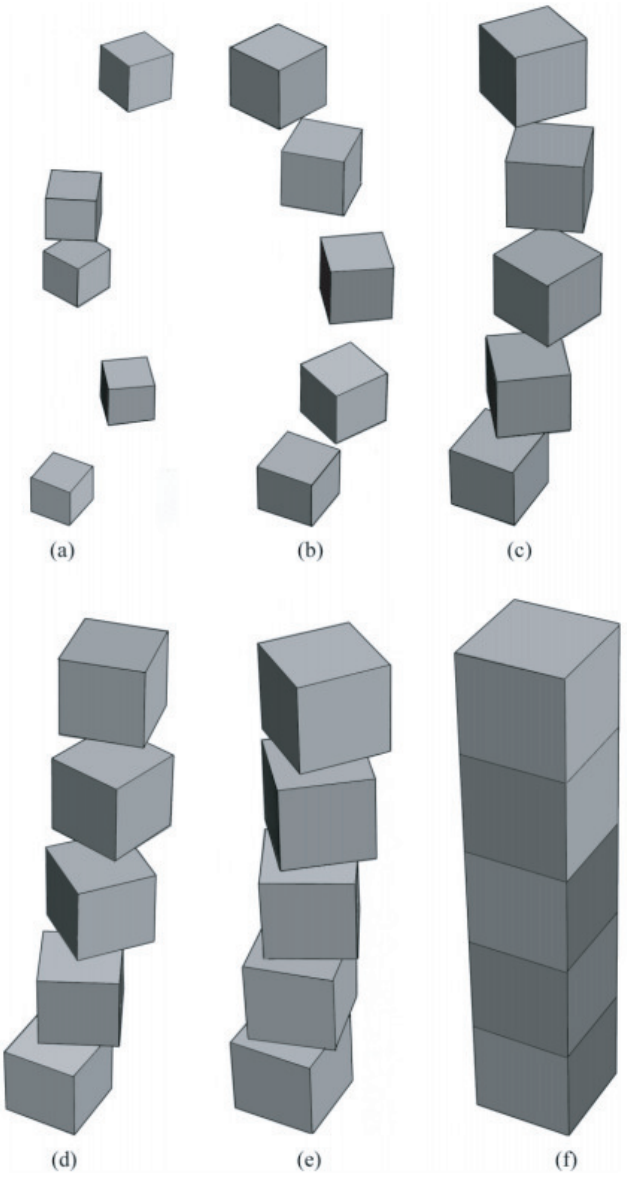

FIGURE 2.9: (a-f) Six stages of assembly for five cubic micritesb, assuming the existance of a potential between pairs of opposing faces Reproduced from [10].

Damsceno et al. [61] and Solem [10] both attempt to describe the results of enthalpic self-assembly when the shape of the module is varied. Solem focuses exclusively on the cube and regular dodecahedron, as out of the Platonic solids they are the only two which have the ability to be packed close together without any gaps- a 100% packing fraction.

He proves that the modules in his assembly (named 'micrites') must be immersed in a fluidic environment in order to ensure that they can assemble, and ideally would also be neutrally buoyant in order for gravity to be neglected. If the existence of a potential is assumed between a pair of opposing figures, the micrites are thought to assemble as in Figure 2.9. If the charged pair of faces is allowed to change in the assembly such that the angle between a pair of micrites varies, then locomotion of the chain is also considered to be possible.

Meanwhile, instead of restricting the number of potential modules to two, Damesceno et al. seek to test as many types of polyhedra as possible in order to analyse how it alters the efficacy of self-assembly. The paper presented here analyses 145 different polyhedra, but the analysis of over $55,000$ different polyhedra [62] has been carried out elsewhere by the same group. They find that, by comparing the *isoperimetric quotient*

$$IQ = \frac{36\pi V^2}{S^3}, \tag{2.1}$$

where V is the volume of the polyhedra and S is surface area, and the *co-ordination number* CN_f is given by the initial local arrangement of the polyhedra within the environment, they can predict the type of crystallised structure the assembled polyhedra will produce under simulation with 94% accuracy.

Finally, van Anders et al. [63] and Randhawa et al. [64] vary the details on specific faces of their modules to see the effects they have on the enthalpy of the system. The former applies an anisotropic force to faces- 'patches'- on a module so that they either specifically or non-specifically interact with patches on other modules, and then varies the size of the patches. Using Monte Carlo simulations, the group demonstrates that changes in patch size alters both the packing fraction and the type of crystal that the modules self-assemble into, for example, from a diamond assembly to a quasi-crystal assembly. Meanwhile, the latter group removed sections from the faces of their modules, to produce patterns with different amounts and locations of the hydrophobic material from which the modules are made. They discover that the patterning which produces an optimal bonding between a pair of modules may not be optimal for a bonding between a single module and an already assembled group of modules. This is highly important in systems where massive amounts of modules are expected to assemble into one cohesive structure. They also produce parameters based on the features of a given pattern which, when optimised, can reduce the level of defects that occur during bonding between modules and groups of modules.

2.3 Summary

From highlighting just a few of the many works on self-assembly, it is clear that each general approach has its own unique benefits and drawbacks. Mechanical self-assembly is often capable of achieving the most geometrically complex structures a.k.a. it has a high level of *addressability*, but due to the number of components required to build each module (motors, electronic communications devices etc.) the modules are generally larger and generally cannot be produced *en masse*. One member of the group that produced the $12mm^3$ Robot Pebbles claimed that it was necessary to learn watchmaking techniques in order to create the internal hardware [65], thus demonstrating the difficulties that would arise if modules the size of a grain of sand using the same Robot Pebble design were attempted. Chemical self-assembly is achievable at smaller scales because the modules do not require small internal components, so it is *scalable*, but the type of structures that can be produced are typically limited to homogeneous patterns and the concept of module addressability has not yet been approached. DNA self-assembly is still growing as a field, but it is generally agreed that only structures at very small scales could realistically be made using the technique. Also, current techniques for producing a self-assembling DNA strand are highly labour intensive. Enthalpic self-assembly has shown considerable theoretical promise but is yet to produce output in physical demonstrations with high impact, where considerations such as gravity and friction cannot be conveniently removed. Lastly, magnetic self-assembly has shown promise in numerous publications but a coherent method in the field for how self-assembly with magnets should be achieved is yet to be concluded upon.

Approach	**Benefit**	**Drawback**
Mechanical	Addressable	Not shown to be scalable
Chemical	Scalable	Not shown to be addressable
Magnetic	Scalable and addressible	Optimal methodology unclear
DNA-based	Addressable	Not shown to be scalable
Enthalpic	Scalable and addressible	Mainly theoretical thus far

TABLE 2.1: Table highlighting the main benefit and drawback for each of the self-assembly approaches discussed in this chapter.

Equally, each general approach highlights the need for self-assembling systems that match the user's requirements. Groups such as NASA are seeking a method to produce a modular robot that can reconfigure based on the goal it is trying to achieve and the robot's environment- this would most likely use a mechanical approach at a large scale [66]. On the opposite end of the spectrum, designing the structure of an artificial virus that can be trusted to react in a specific way when it encounters an abnormality in the human body is a way in which DNA self-assembly could be employed.

Two fundamentally different techniques are required for producing the systems in the examples presented in the paragraph above, and there are many more problems which exemplify that the existence of a grand unifying method for solving all self-assembly problems could well not exist. Further, although there have been self-assembly projects which overlap significantly in terms of the methods used, very little fundamental theory has been developed which can then be built upon in subsequent studies. It is the hope of the author that this work will present some new, fundamental theory in the field from which other groups can establish their own work. Only by producing stepping stone-like research such as this can a distant goal of the ideal self-assembling system, where minuscule modules work in harmony to produce any object the human desires, be rendered achievable.

Chapter 3

The Challenge

This chapter will attempt to distil the concepts that appear to be the most successful from the literature and from nature, in order to devise a method and hypothesis for producing a self-assembling system that is capable of overcoming some of the issues that have arisen in previous work.

In the previous chapter it was made clear that self-assembly approaches with mechanical and electronic components as the main source of automation have inherent problems during experimentation. It would not be too difficult to produce a module that contains separate systems for locomotion and communication, for example by using a set of wheels, a motor, a battery, and some sort of signalling device. The issue is that this module would be so large as to be considered a robot in its own right, with the ability to collaborate with other robots in a swarm-like fashion, contradicting the condition of 'emergence' utilised in Chapter 2. The ultimate goal in self-assembly is for each module to be so small that the structure they produce does not appear to have granularity. This means that, by developing a system which requires all of these components in order to function, one is implicitly assuming that batteries, signalling devices etc. will all at some point in the future be manufactured at the nano- or even micro-scale. Although this may indeed be the case, this is likely to be at least several decades ahead from now and as such this assumption stalls the capability for many current self-assembly approaches to produce an impactful result. Furthermore, each of these components could be considered a module in its own right as they are each typically composed of several smaller parts. Therefore, any module fabricated using these components could also be considered a meta-module. This situation should ideally be avoided because each module should be capable of being treated as a 'building block' from which other structures are made, rather than a structure in its own right.

3.1 Anfinsen's Dogma/ Thermodynamic Hypothesis

Although the process of using DNA to directly self-assemble structures has deliberately not been covered in depth in this work, the approach of mimicking the techniques used in biological self-assembling systems may well be the most useful - after all, it is a process capable of creating vastly complicated creatures, while the successes of artificial self-assembly are orders of magnitude smaller. It therefore seems that there is still much to learn pertaining to self-assembly in nature.

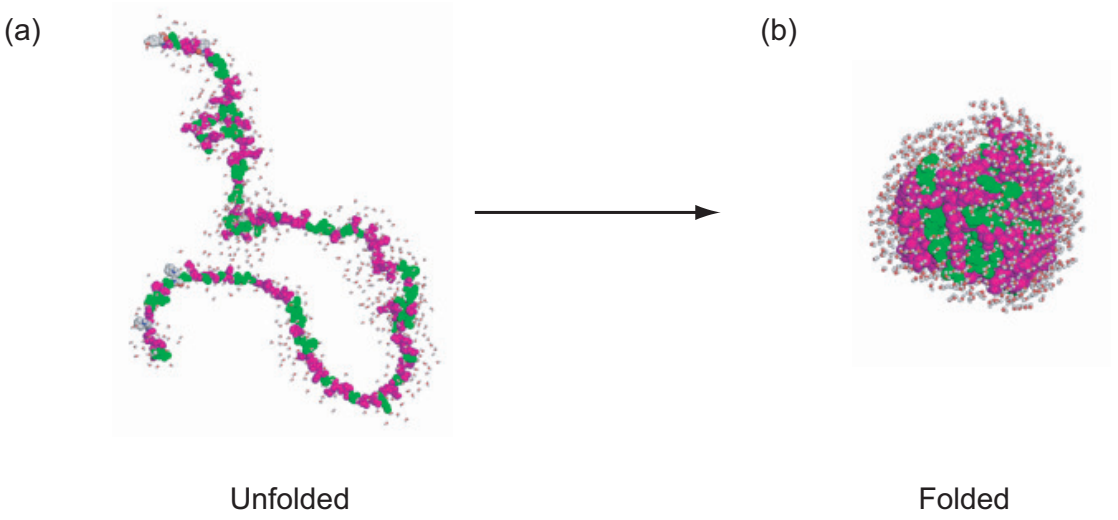

FIGURE 3.1: Folding of a protein chain. (a) Protein chain in unfolded state. (b) Protein chain in folded state. Adapted from [11].

One theory, postulated by Christian B. Anfinsen in 1973 [67], gave rise to a new type of understanding about the methods proteins use to fold into their native (folded) state (see Figure 3.1 above). By repeatedly denaturing and renaturing a protein, Anfinsen demonstrated that all the necessary information required for a protein to fold properly is stored within its amino acid sequence and not within its environment. This statement, known equally as *Anfinsen's Dogma* or the *Thermodynamic Hypothesis*, has since found some exceptions (prions, and proteins which require molecular chaperones to fold successfully [68]) but is still held as a fundamental theory in molecular biology. It would therefore be reasonable to suggest that an artificial system should also strive to not rely on its environment for directing how it should fold, which removes from consideration some of the methods discussed in the previous chapter. In addition, since all of the tools needed to fold the protein are contained within one type of organic compound (the amino acid), a system inspired by protein folding should be designed such that tools for folding are composed of as few different types of components as possible - for example, using one device for both locomotion and communication between modules instead of two.

Anfinsen also stated three conditions which the native state of a protein must fulfil. These are:

1. Uniqueness- The free energy of the native state must be lower than the free energy of any other possible protein state.

2. Stability - The native state is resilient to small perturbations. In other words, the energy landscape of the system must be 'funnel' shaped around the location of the native state [12].

3. Kinetical Accessibility- The journey of a protein from its initial state to its native state must not contain any higher-order transitions, for example it must not contain a knot.

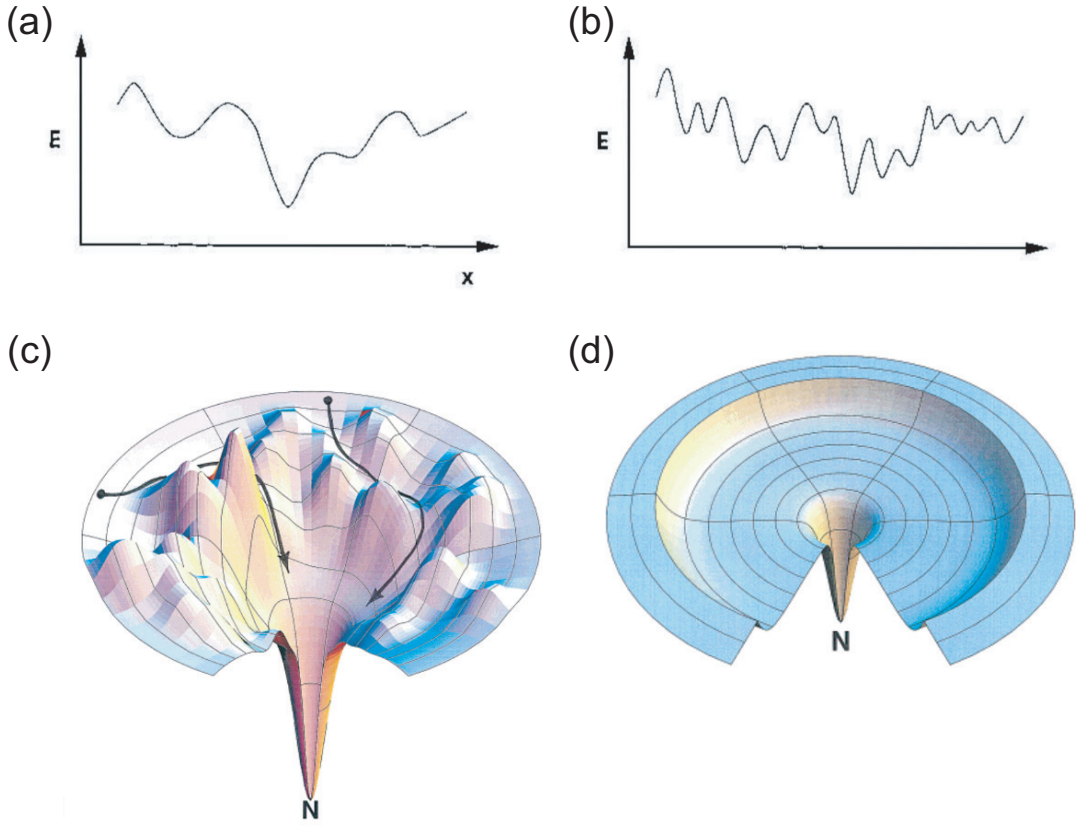

FIGURE 3.2: Examples of energy landscapes. (a) A smooth energy landscape containing broad funnels leading to a few energy minima. (b) A rough energy landscape with narrow funnels leading to many energy minima. Both reproduced from [12]. (c) An energy landscape portrayed in three dimensions, with native state N. A and B are candidate paths through the energy landscape which the protein can follow. (d) An energy landscape containing a 'bottleneck', where the level of energy in the system remains constant. This will slow down or prevent the protein from reaching N. Reproduced from [13].

These conditions all centre around the idea of *enthalpy* with regards to the protein: beginning the denaturing process with the largest amount of energy, and monotonically dissipating energy until the final state is reached. This is comparable to Whitesides and Grzybowski's definitions of static and dynamic self-assembly discussed earlier. The folding of a protein would be equivalent to cases of passive self-assembly, thus indicating that passive self-assembly may be preferable when deciding on the criteria for this work. This removes from consideration many of the previous techniques that have relied on environments containing shakers, electromagnetic coils etc. to provide the systems with a continuous source of energy.

3.2 Energy Landscaping

It is desirable to utilise all three of Anfinsen's conditions within artificial self-assembly. A system that fulfils all three conditions would simply and reliably reach its final shape without requiring any external influence, and then would stably remain in its final state. However, there exists no robust process for engineering a system such that its natural final state aligns with the final state desired by the user. One caveat of Anfinsen's paper is that, if a protein's natural state is always its global energetic minimum, the protein must look through an enormous search space of conformational states in order to be certain that it is in fact the global minimum. Levinthal [69] first documented this problem even before Anfinsen's publication, and it is thus known as *Levinthal's Paradox*. Unger and Moult [70] have since proved that the task of searching for the lowest free-energy structure for a protein is an NP-hard problem, meaning that it most likely cannot be solved in polynomial time.

One method for overcoming this issue would be to physically restrict the the search space such that there are fewer choices as to how the free energy of the system can be reduced. Consider a system of modules that utilises permanent magnets. If the magnets were left to move completely freely, they would clump together or form a chain end-to-end due to their respective magnetic forces. However, if the magnets were restricted in their movement by walls, they would still attract or repel each other but within the physical constraints of the walls. By increasing the level of restriction imposed by the walls, a direct corridor to the lowest available energy minimum can be created. The lowest available energy minimum can then be specified such that it produces the desired final outcome of the system. This is an example of a theoretical method used in biology and physical chemistry known as *energy landscaping* [71] [72]. An equivalent in biology would be a protein strand attempting to reach its native state inside an environment designed to block the majority of its movement - it will reach the energy minimum that

it is able to reach, and no more. It will be seen that this theory underpins the work that will be presented in the following chapters.

3.3 Summary

From the above discussion it is possible to derive the list of 'design criteria' used for the system presented in this work. These are:

- Minimise reliance on mechanical, electronic or chemical approaches for self-assembly
- Use concepts from literature on magnetic and enthalpic approaches to self-assembly
- Seek to replicate an existing biological self-assembling system - the folding of a protein chain
- Minimise the number of distinct module components
- Fulfil the three conditions of Anfinsen's dogma: Uniqueness, Stability, and Kinetical Accessibility
- Use a method of passive self-assembly
- Restrict the available energetic states of the system so that its global energy minimum corresponds to the global energy minimum of the desired final state

Some non-essential (but desirable) design criteria were also added during the development process, for example the requirement that the modules are not permanently physically connected. The reasoning behind these extra criteria will be explained as they arise.

The hypothesis of the project can also now be stated: By taking inspiration from the theories described above and by not relying on mechanical and electronic components in the fabrication process, it will be possible to produce a system capable of both locomotion and communication that can be scaled downwards in terms of size and upwards in terms of module numbers without the need for a paradigm shift in system design.

Chapter 4

Design Series I

This section contains a description of the publication most closely related to this project, along with a description of the first main design iteration. Although there are fundamental differences between the final design presented in this dissertation and the previous design iteration, an exploration of the previous design iteration is useful as a grounding for some of the choices made in the final design.

4.1 Main Design Motivation

The main source of motivation for this project was the paper 'Mechanical Catalysis on the Centimetre Scale' by Miyashita et al. published in 2015. In this paper, pairs of 3D-printed tiles containing magnets were floated on water along with individual free-floating magnets named 'enzymes'. If an enzyme entered within a certain distance of one of the two magnets in the tile, it would trigger the reconfiguration of the magnets in the tiles, resulting in another magnet being released into the water that could then serve as an enzyme for other pairs of tiles.

All magnets in the system are placed with their poles perpendicular to the surface of the water so that they can be considered as dipoles. Magnets with opposite poles pointing upwards attract each other while those with the same poles pointing upwards repel each other. Inside the tiles, the magnets M1 and M2 in Figure 4.1 are attracted to each other but initially cannot move towards each other due to the 'hook' shape in the path of M2. The enzyme (referred to as M3) is attracted to M2 and can float towards M2 until it reaches the perimeter of the tile (phase k_1). Once the enzyme is within a certain distance of M2, M2 can also begin to move towards the enzyme (phase k_{2-1}). Both magnets then slide in the direction of M1 due to the monotonically decreasing distance

between the edge of the tile and the path of M2. Once M2 reaches the end of this section of the path, the distance between M1 and M2 is smaller than the distance between M2 and the enzyme, and thus the now stronger attraction between M2 and M1 causes them to continue moving towards each other while both moving away from the enzyme (phase k_{2-2}). After they have moved towards each other for a certain distance the enzyme is no longer within the region of attraction of M2 and is free to float away from the edge of the tile (phase k_3). The enzyme could then trigger the reconfiguration of magnets inside other available pairs of tiles. Meanwhile, M1 and M2 cause the tiles to rotate and change their configuration, while triggering the release of a third magnet which can also float away from the tiles and serve as an enzyme. Alternatively, if an inhibitor is attracted to M1 rather than an enzyme, the movement of M1 towards M2 will be blocked and the tiles will not change their conformation.

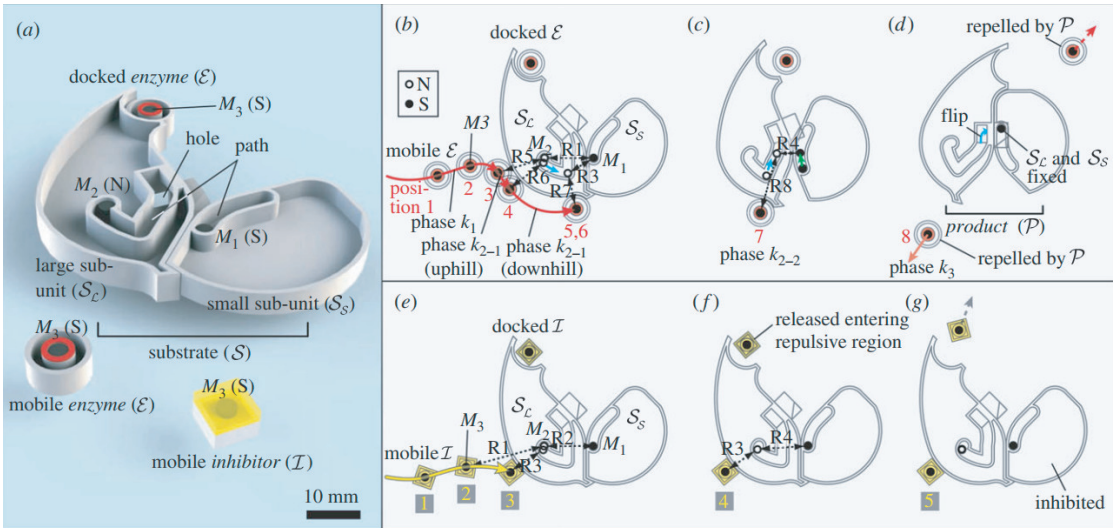

FIGURE 4.1: Self-assembly system, reproduced from [14]. (a) Physical overview of units. (b)-(d) Magnetic catalysis causing a conformation change. (e)-(g) Inhibition of the conformation change.

4.2 The Transition Diagram

The key design consideration for the system described above is the relative distances between the magnets in each stage. In order for a magnet to be moving, there must be a magnetic attractive force acting on it in one direction more than any other direction, and the magnet's path in that direction must not be obstructed. An obstruction that provides an energy threshold for when magnets can begin moving towards each other is referred to in Fig. 4.2 as the 'activation potential'. Also, the distance between two magnets that are attracted to each other must be decreasing monotonically, otherwise the movement of the magnets would come to a halt. This can be more easily understood

through the use of a 'transition diagram'. Each line in the diagram represents one magnet, and the distances between the lines indicate the respective distances between the magnets at that point in the system. It should be noted that, although the lines indicating movement in the diagram are linear, the actual velocities of the magnets are generally non-linear.

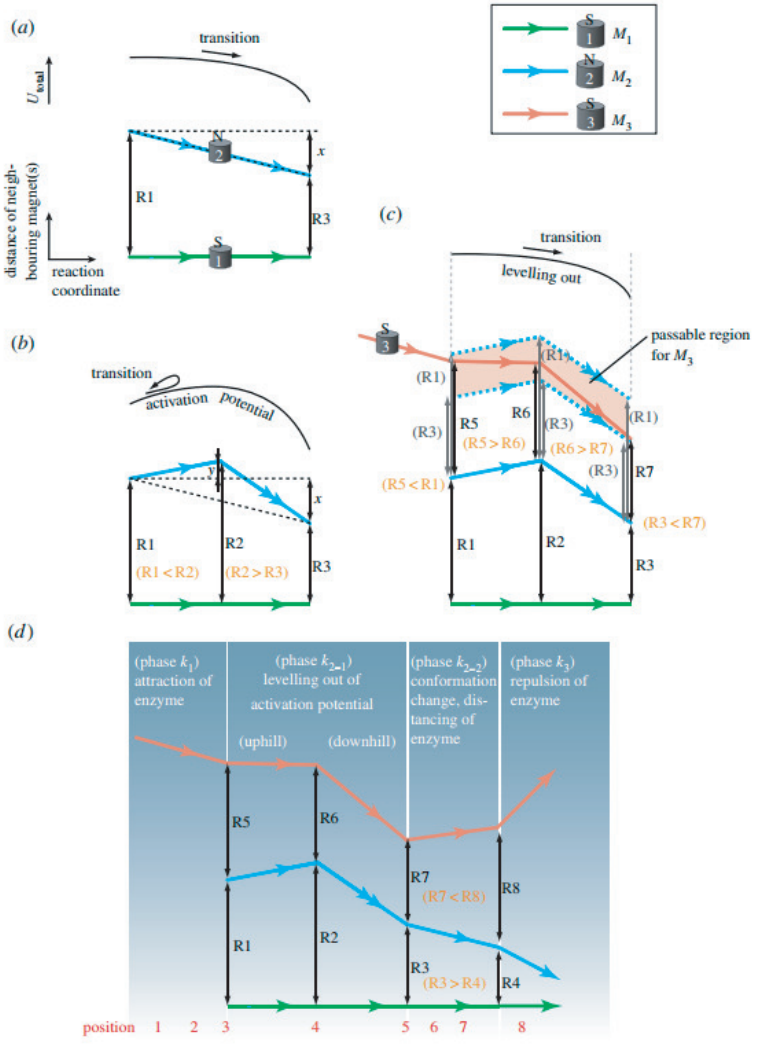

FIGURE 4.2: Incremental design of the enzymatic process. (a) Sliding motion of magnets. (b) Activation potential that is obstructing the movement of a magnet. (c) Magnetic catalysis. A third magnet M3 escorts M2 over the activation potential barrier and allows it to continue moving. The distances displayed are labelled in parentheses. M3 must pass through the entire pink region for successful catalysis. (d) Transition diagram for the conformation change system shown in Fig. 4.1. Reproduced from [14].

For the system described in this previous paper, the transition diagram would end here as the tiles have reconfigured and all magnets remaining in the system are stationary. The challenge presented at the beginning of this project was to produce a system in which the transition diagram could be extended to include an arbitrary number of tiles.

4.3 First Design Series

The system following on from the previous publication is influenced by currently unpublished research carried out by Valentin Besnard (see [73] throughout for details of their work), and works as follows: 3D-printed tiles containing one or two magnets each are floated on water. The magnets in the tiles attract each other enough for the tiles to form a chain but the tiles are not physically linked together. The magnets are held in position by walled paths inside the tiles. When a lone magnet is floated towards a specific region of the first tile in the chain, a catalytic reaction is triggered within the magnets such that they sequentially reconfigure all the way along the chain. Depending on the type of path which holds the magnets (there are a finite number of path types), 90° folds can be produced in the chain and thus cause the overall shape of the chain to change. It should be possible to produce a wide variety of 2D designs by choosing the locations of tiles containing paths that produce folds in the chain.

The figure below shows a system comprising two tiles as viewed from above. M2 and M3 are attracted to each other, but cannot move towards each other due to the shape of the paths holding them in place (Stage (a)). In order for M2 to begin moving, an external magnet (the enzyme) must approach M2 from such a direction that the distance between M2 and the enzyme can be smaller than the distance between M2 and M3 (Stage (b)). If not, the enzyme will be fixed at the edge of the tile but will not induce any catalytic reaction in the system.

Once the enzyme is in the region of attraction for M2, M2 will move towards it until the path walls impede its movement once more (Stage (c)). However, due to the curved nature of that section of path wall and the fact that the enzyme is not physically constrained, M2 and the enzyme can continue to decrease the distance between each other if the enzyme rolls down the outer edge of the tile slightly. It is at this point where the distance between M2 and M3 becomes smaller than the distance between M2 and the enzyme and so the attraction between M2 and M3 becomes dominant (Stage (d)). M2 and M3 can continue to approach each other by moving across the tile and away from the enzyme. After a certain distance has been covered, the attraction between M2 and the enzyme will be so weak that the enzyme will float away (Stage (e)). Once M2 and M3 have moved past the hinge between the tiles, the force between them is enough for the tiles to rotate about the hinge to produce a fold in the chain (Stage (f)). The external tile walls are chosen such that all folds will produce a 90° angle, for ease of design (although this could be relaxed in future designs). Finally, M2 and M3 continue to move towards each other until they reach the end of their respective paths (Stage (g)). This is partially to 'lock' the new folded tile into position, but its main purpose is to move M3 closer to M4. This is because, if the chain consisted of three or more tiles,

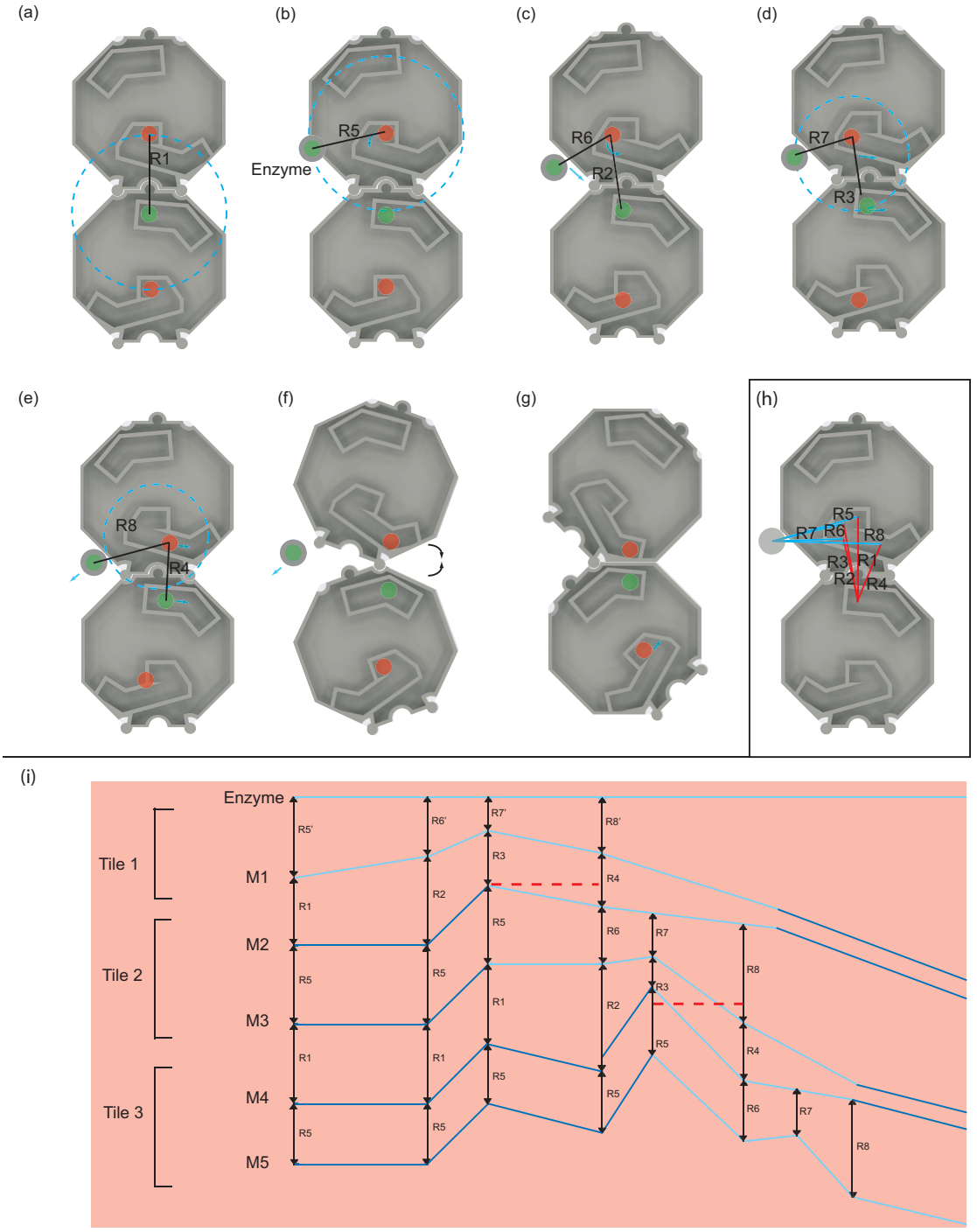

FIGURE 4.3: Figure showing stages of design first proposed by Valentin Besnard and the further developed by the author. (a) Initial system, M1 and M2 are closer together than M2 and M3, but cannot approach each other. (b) Enzyme approaches the system from the correct side. (c) M1 is pulled towards the enzyme once it is within range. (d) Relative distances change such that now M1 and M2 are closer to each other, and can also approach each other. (e) M1 and M2 move sideways across the tile, increasing the distance between M1 and the enzyme, until the enzyme floats away. (f) M1 and M2 move past the hinge point to produce a folding torque. (g) M2 acts as an enzyme and starts the motion of M3. (h) Locations of all important distances during phases $R1$ to $R8$. (i) Transition diagram for the first few tiles of an extended version of this system, much like an extension of the transition diagram shown in Fig. 4.2. Light blue lines indicate relative distances of magnets that are moving relative to the tiles on which they are situated, dark blue lines indicate that they are static. Red dashed lines indicate where tiles would fold.

M3 would need to play the role of the enzyme to initialise the movement of M4, and so needs to be close enough to M4 for it to trigger its movement in the same way that the enzyme does for M1.

Miyashita et al. [14] were able to produce a system of inequalities based on the distances between magnets at different actuation stages, which ensures the success of magnetic catalysis for this type of system. The distances translated into this new type of tile design are shown throughout Fig. 4.3(a)-(g) and collected together in Fig. 4.3(h), while the inequalities with respect to these distances are:

$$R3 < R7 < R6 < R5 < R1 < R2 \tag{4.1}$$

$$R4 < R3 \tag{4.2}$$

$$R7 < R8. \tag{4.3}$$

Eq. 4.1 enables magnetic catalysis, Eq. 4.2 enables the conformation change and Eq. 4.3 enables enzyme repulsion. Finally, the transition diagram for the system is shown in Fig. 4.3(i). A system composed of three tiles is shown here, although in theory an endless chain of reconfigurable tiles could be made in this way.

4.4 Second Iteration of Design

Although the prospect of an endless chain of tiles reconfiguring with one initial energetic input is exciting, there is a caveat to this type of system in terms of the potential shapes that the chain can form. The first iteration of this type of design (carried out by Valentin Besnard) assumed that a 90° fold would occur between every tile. However, from the figure below one can see that issues due to collision would soon arise in this kind of system (further details in Chapter 5). Such a reduction in universality of the system was a major issue and weakened findings significantly.

The next iteration was very closely related to the previous design but was intended to not produce a folding motion between every tile. This was to be achieved by finishing the paths slightly earlier so that they do not pass the hinge point of the tiles, while still allowing magnets in adjacent tiles to be close enough to trigger catalysis down the chain (see Figure 4.5).

It is clear from this description that the geometry of the paths must be precisely designed to control the movement of the magnets. In order for two magnets to continue moving,

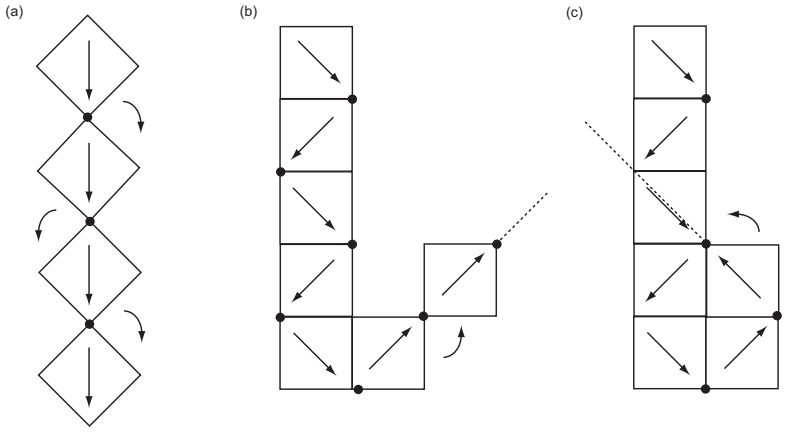

FIGURE 4.4: The collision problem in the first design iteration. (a) Schematic of the tile chain in its initial state. Arrows inside the tiles denote orientation. Curved arrows outside the tiles denote the direction of folding. (b) Chain during the folding process. Dashed line indicates continuation of the chain. (c) Collision occurs during folding at this stage of actuation.

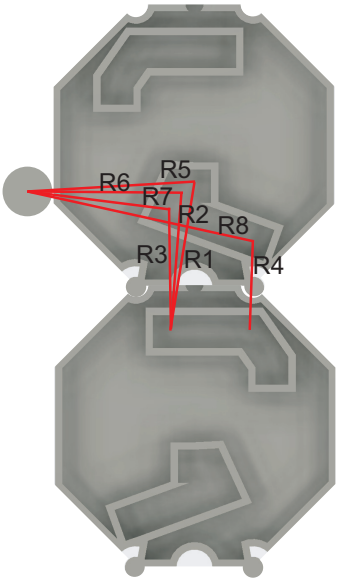

FIGURE 4.5: Next iteration of Miyashita-type design. (a) Diagram of the tiles with important distances labelled. (b) A table of the lengths for each distance. Some pairs of distances (such as $R3$ and $R4$) are so similar in size that the potential energy gradient is close to zero and the magnets cannot continue travelling along the path.

the distance between them must decrease strictly monotonically. In a theoretical model where forces such as mass or friction are not considered, a pair of magnets will slide towards each other if their paths are approaching each other incredibly slowly i.e. the angle between the paths is $\frac{\pi}{2} - \epsilon$, $\epsilon << 1$, but this is not the case in a physical model: a force on a real magnet must overcome the static friction between the bottom of the magnet and the tile as well as any forces being applied by other magnets. For this reason, any two paths that are approaching each other must also approach at a sufficiently large angle for these forces to be accounted for.

Name	Distance (mm)
R1	13
R2	17.5
R3	18
R4	18.215
R5	18.627
R6	20.314
R7	20.5
R8	30.282

TABLE 4.1: Table of the lengths corresponding to each distance in Figure 4.5. Some pairs of distances (such as $R3$ and $R4$) are so similar in size that the potential energy gradient is close to zero and the magnets cannot continue moving along their respective paths.

Similarly, the differences between distances given in Equations 4.1-4.3 must be sufficiently distinct in physical models to account for other forces present. In theoretical models, the decision of whether Magnet B will move towards Magnet A or Magnet C is purely binary- Magnet B will move towards whichever magnet is closer, regardless of how large or similar in length those distances are. In reality, Magnet B would only begin to move if the magnet was sufficiently close both objectively and relative to any other magnets in the environment. When analysing the distances given in the inequality, it soon becomes apparent that the importance of relative distance is a source of difficulty for designing a tile of this type.

Looking back at equations 4.1-4.3, it can be seen that R1-R3 are the distances between the enzyme and the first magnet within the first tile. R2 is the largest distance in Equation 4.1, but then must decrease in size to become the second smallest distance, R3. Further, The pairs of inequalities

$$R3 < R7,\ R6 < R2,\ R5 < R1 \tag{4.4}$$

derived from Equation 4.1 are inextricably linked: reducing the length of one distance will increase the other in the pair (with the exception of moving the point at which the two lengths meets along the loci between the magnets). For example, the distance R3 is decreased, R7 will consequently increase and further restrict the possible values that the other distances can take. Table 4.1 details the lengths for the distances in one of the prototype tiles. The distances match the rules imposed by the inequality but catalysis was not successful in simulation (see Appendix A). This is because, although all of the distances match the inequality, some are only separated by fractions of millimetres. This is a good example of the issues discussed above, where a theoretically successful model does not translate to a successful model in simulation or in physical experiments.

4.5 Summary

The fact that this first design did not produce a successful result at this stage does not mean that it will never be successful. It is possible that future platforms that are able to reduce influences such as mass and friction would be able to produce successful results using the design, and it is for this reason that documenting the research carried out here is important. At this stage in the current project, it was decided to try a subtly different approach to achieve the desired results, while being aware that the first design could be revisited in the future.

Chapter 5

A Review of Collision Algorithms for Folding Chains

Development of the design iteration discussed in the previous chapter was suspended due to the chain self-intersecting during the configuration process. This problem is a well-researched area in both mathematics and biology. The following section will present some of the main ideas and theories regarding collisions during folding, and will summarise with the strategy adopted for avoiding folding collisions in the design iteration covered in this thesis.

5.1 The Hamiltonian Path Problem

The aim of this work is for the chain to approximate a 2D shape by filling the shape with tiles in a chain. All tiles in the chain are initially positioned in a straight line. The chain must fold into an approximation of the shape by folding a finite number of times. As the chain cannot break apart, the problem of finding a folding sequence for the chain can be considered as a Hamiltonian path problem; that is, by converting the inside of the shape into a grid with a vertex at the centre of each grid unit, the chain must find a path through the grid which visits each vertex exactly once. Determining whether a graph contains a Hamiltonian path has been proven to be a NP-complete problem [74]. This means that, although it is relatively simple to verify that a given path through the grid is Hamiltonian, finding a Hamiltonian path in the first place is computationally prohibitive.

Cheung, Demaine et al. [15] have produced a method for which any graph can be converted into a graph that contains a Hamiltonian circuit (a Hamiltonian path that begins

and ends at the same vertex). The method generally involves splitting each unit of the grid into four, so the universality of this approach is at the cost of increased size of the final, folded shape. The method can also be extended to three dimensions. According to their publication, "There exists a subset of constructions for many (perhaps all) figures that produce non-self-interfering folding, when folded sequentially. Future work will explore whether this is also true for folding in parallel". 'Self-interfering' is taken to mean the collision between parts of the chain during folding and will be used alongside 'self-intersecting'; 'sequentially' is taken to mean that each fold is carried out one at a time but not necessarily in order from one end of a chain to the other. An algorithm corresponding to Demaine's research [75], which would determine the folding sequence for a chain in any configuration to fold into any other configuration, is yet to be established. However, the existence of a continuous, non-self-interfering motion between a linear chain and any path that has been planned using the method described above has already been proven (see Figure 5.1). In terms of reconfiguration, a folded chain in any configuration A can be re-folded into any configuration B with a continuous, non-self-intersecting motion.

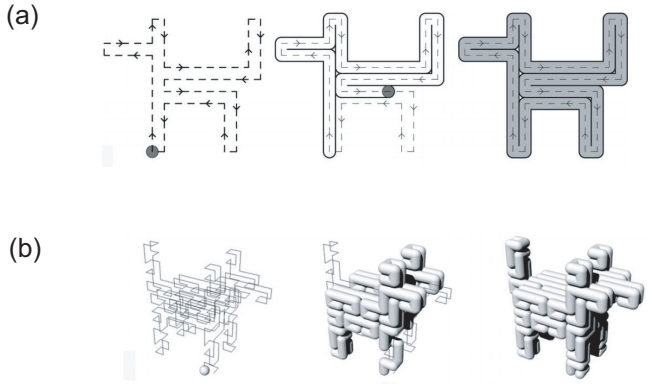

FIGURE 5.1: Chain folding sequences for a 'dog' shape using a Hamiltonian path. (a) 2D chain folding sequence. (b) 3D chain folding sequence. Reproduced from [15].

When experimenting with simultaneous folding in the physical system described above, the authors found that folds at extremities of the chain tended to be completed earlier than those towards the chain's centre. This was due to inertia in the system. Therefore, even if the system was considered to be one of parallel/simultaneous folding, issues of self-intersection that arise in sequential systems would still need to be considered. They also calculated the upper time limit for a folding system composed of n tiles- $O(n^{3/2})$ for parallel folding and $O(n^{5/2})$ for serial folding.

Yim and Sitti [6] investigated Hamiltonian path planning for a 3D shape by splitting it into layers of 2D shapes. Folding happens simultaneously within a layer, and begins in the next layer only when all of the folds in the previous layer are complete. They produced two algorithms for producing the path design, the 'inner connection method'

and the 'boundary connection method' (see Figure 5.2). A combination of these two methods could be employed in the same layer if necessary. Paths for convex and concave shapes, as well as shapes containing holes, were successfully planned using this method.

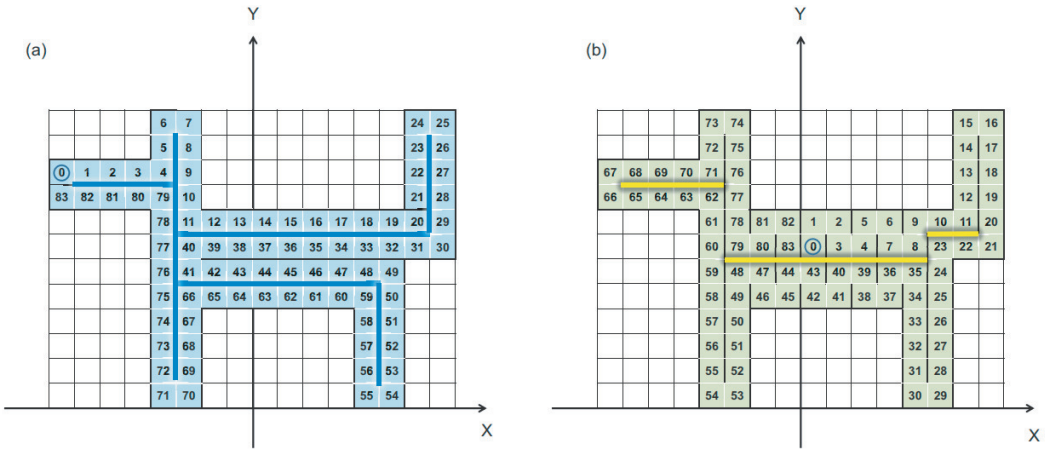

FIGURE 5.2: Candidate paths for creating a 'dog' shape. Paths start at 0 and move in increasing numerical order. (a) 2D chain folding sequence constructed from two Hamiltonian paths connected together. (b) 2D chain folding sequence constructed using the 'inner connection method'. Reproduced from [6].

5.2 The Carpenter's Rule Theorem

The problem of folding order is also related to a sub-problem of the Carpenter's Rule Problem: can any non-self-intersecting polygonal chain be straightened with a continuous transformation that preserves edge distances and avoids crossings? This was proven to be true by Connelly et al. [76], and thus it is known that a folded chain can unfold into a linear chain, with all folded parts unfolding at the same time and not halting at any point. However, the unfolding speed for each hinge point is not specified and could vary throughout reconfiguration of the system.

Streinu [77] gives an algorithmic solution to the Carpenter's Rule Problem with sequential unfolding of the system into a chain- the resulting sequence could simply be reversed for sequential folding. The proof and resulting algorithm are rather technical and include techniques from Rigidity Theory, Visibility graphs, and Oriented Matroid Theory.

5.3 Algorithmic Solutions

The SOftware Library for Interference Detection, or SOLID [78], checks for collisions during the deformation of rigid bodies by performing intersection tests constantly throughout a simulation. This is similar to the method used in many gaming physics engines. Using a library such as this would allow verification of whether a given set of folding orders and speeds resulted in a collision or not, but would not produce the set of folding orders itself. There are countless examples in the literature of collision detection algorithms for both concave and convex shapes- one summary is given here [79]. Of particular note is a paper by Agarwal et al. [80], where the case of collisions between polygons whose shapes continually change over time is considered.

An interesting practical subset of research for this problem is that of sheet-metal bending: collisions are not permissible during the bending process, and generally a sheet of metal can only be bent sequentially and from one end of the sheet to the other. Computer-aided process planning (CAPP) systems are typically used to solve this problem algorithmically. According to Vin et al. [81], for a system containing n bending points and m different folding angles, there are $n! \times mn$ different possible configurations without taking collisions into account. In particular, Arkin et al. [16] give an algorithm for determining the foldability of a chain into the chosen shape using a sequential strategy, where each hinge point is straightened in order along the chain and each hinge can only be manipulated once. Furthermore, they provide extensions for cases where folds occur from both ends of the chain inwards or from the chain's centre outwards.

A brief description of the algorithm is as follows: For a chain made of n tiles there will be $n-1$ joints to check. When the chain is fully unfolded all of the joints will be straight. Begin from one end of the chain and check each joint in turn. If the joint is already straight then move onto the next joint. If the joint is not already straight, attempt to straighten it without any part of the chain colliding with itself (confirming this using ray-shooting and wedge emptiness queries). If the $n-1^{th}$ joint is reached and successfully straightened, then the chain can be unfolded and equally the chain can be folded from a straight initial configuration to this final design. The algorithm can be completed in $O(n\log(2n))$ time. It would be necessary to choose methods for the ray shooting and wedge emptiness query parts of the algorithm, of which there are many.

5.4 Forward and Inverse Problems

Current research can be placed under the headings of two questions:

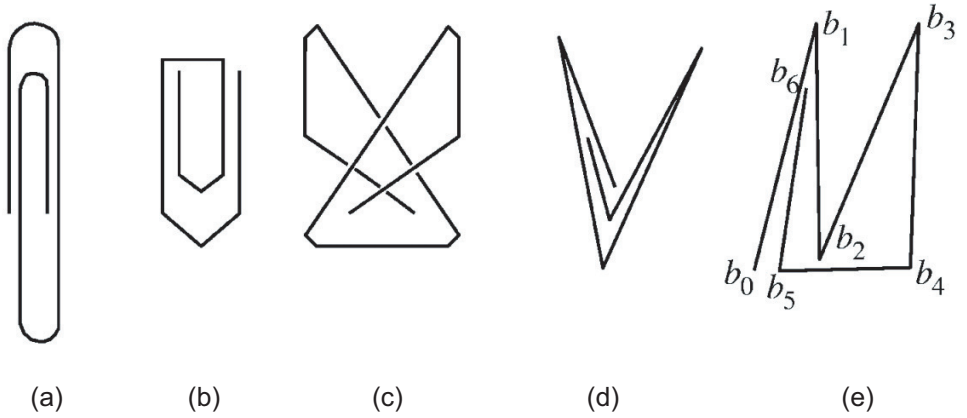

FIGURE 5.3: Examples of folded structures. (a), (b) and (e) can be unfolded without intersection. (c) is self-intersecting in its final state. (d) cannot be sequentially unfolded without causing a self-intersection. Reproduced from [16].

1. Given a chain that has been folded, has it self-intersected during the folding process?

2. Given a chain in its unfolded state, what shapes can be made by folding the chain while not causing any self-intersections?

These can be thought of as the *Inverse Problem* and the *Forward Problem*, respectively.

The system presented in this paper is a set of tiles in a chain formation, starting at one end of the chain and folding sequentially until the other end of the chain is reached. With respect to this system, the Inverse Problem is considerably more straightforward to approach than the Forward Problem as the answer to the Inverse Problem is simply 'Yes' or 'No'. An algorithm similar to that described in [81] could be employed to determine whether or not a folded chain can be unfolded without causing an intersection. In contrast to this, much less can be said about solutions to the Forward Problem.

Consider a chain composed of n tiles. There will be $n-1$ joints between the tiles. In the system presented in the following chapter there are three possible choices available at each joint: Fold 90° to the left, fold 90° to the right, or do not fold. Thus, without taking any issues of self-intersection into account, there will be 3^{n-1} candidate configurations for each chain. It is then possible to remove self-intersecting configurations from the list of candidates. For example, a run of three consecutive left turns or right turns will cause a self-intersection for chains longer than 4 tiles in length. Further, if three left or three right turns T_{ab}, T_{bc} and T_{cd} are carried out with only sequences of consecutive non-folding joints between them of lengths a, b, c and d, respectively, then it is necessary that $d < b$ or $a < c$ (or both) in order for self-intersection to be avoided (see Figure 5.4). There is no complete formula as of yet to determine exactly how many non-self

intersecting configurations are possible for a chain of arbitrary length, but, simply from testing some small examples, it is clear that a large amount of candidate configurations can be removed due to self-intersection occurring either at the final state or during the self-folding process.

No. of Tiles	Candidate Configurations	Successful Configurations
2	3	3
3	9	7
4	27	17
5	81	35
6	243	79

TABLE 5.1: Table comparing the number of candidate configurations to the number of non-self intersecting configurations. Note that, for the current version of this system, consecutive 90° turns in opposite directions are not utilised.

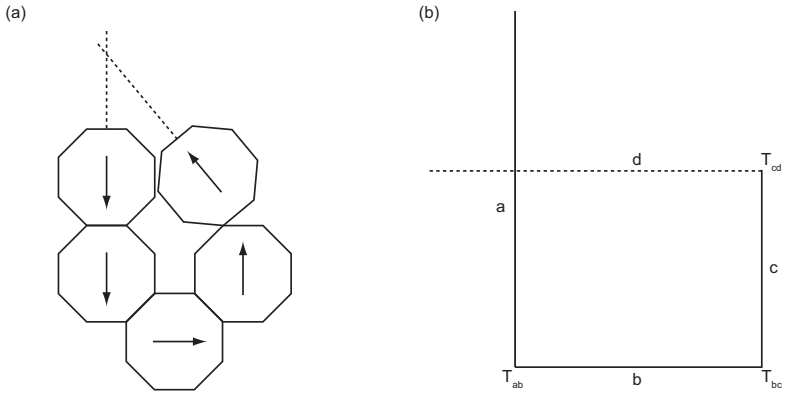

FIGURE 5.4: Examples of non-allowable configurations. (a) Three consecutive left or right turns will cause a collision if they are not the final three joins in the chain. (b) Schematic of another collision type, where three left or right turns are separated only by straight sections of chain. Already configured chain is represented by a solid line while the part of chain still to be configured is represented by a dashed line.

5.5 Configurable Shapes

Finally, it is useful to be able to know instantly whether a given shape can be filled using only the 90° turns provided by tiles in the present system. Two consecutive 90° turns can be used to produce a 180° turn clockwise or counter-clockwise. Different shapes can be filled in by alternating the direction of the 180° turns and separating them with varying lengths of non-folding sections of tile chain (see Figure 5.5).

It is clear that all convex shapes can be filled using this method, with accuracy dependent on the size of the shape to be approximated. However, certain other shapes can also be produced using this method. In computational geometry, a polygon is said to be *monotone with respect to a line* L, if lines orthogonal to L intersect L at most twice [82].

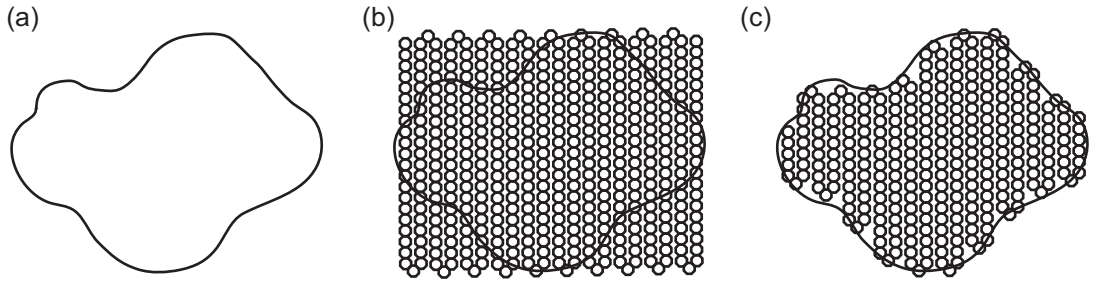

FIGURE 5.5: Method for filling a shape using a tile chain. (a) Initial shape to be filled. (b) Amount of clockwise and counter-clockwise turns needed to fill the shape is calculated. (c) Length of straight sections needed to fill the shape is calculated depending on target shape and tile sizes. Note that a higher resolution approximation to the shape can be made, at the cost of a larger final shape and increased amount of tiles.

For example, the polygon in Figure 5.6 is monotone in 5.6(a) but non-monotone in 5.6(b). The shape can therefore be folded provided that folding is carried out using specific orientations, of which 5.6(a) is an example. Therefore, the chain can also be folded to approximate concave shapes, as long as they have a line to which they are monotone. Finally, some other shapes can be folded if 90° turns are interspersed with the 180° turns. An example of a 'key' shape using a single 90° turn is given in Figure 5.6(c).

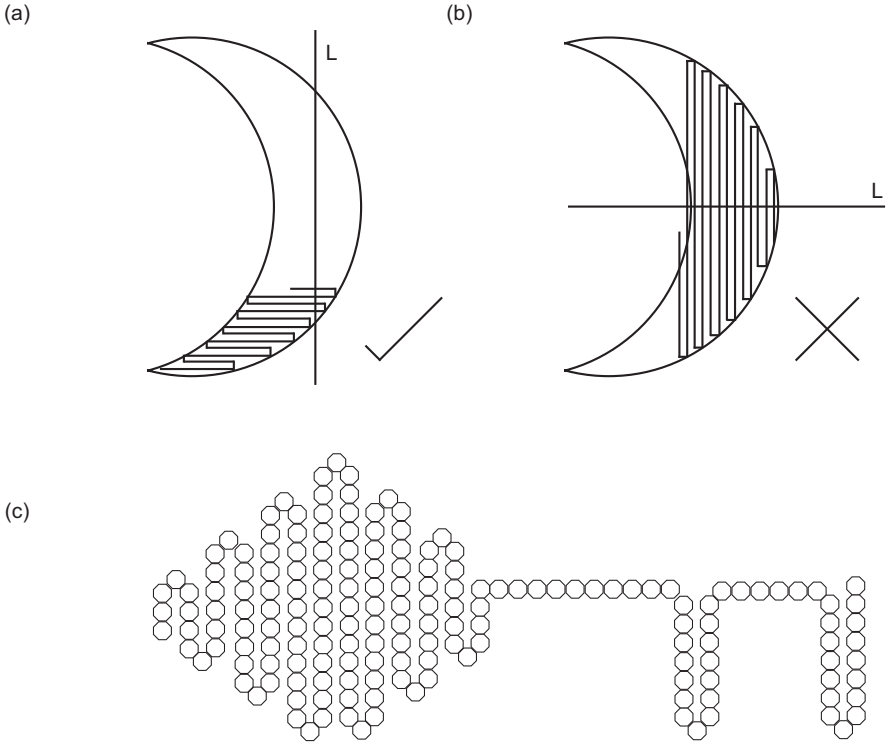

FIGURE 5.6: Examples of how the chain can be folded to produce shapes. (a) A crescent shape can be folded when a vertical folding axis is used. (b) The same crescent shape cannot be folded if the folding axis is horizontal. (c) A key shape produced using a combination of 90° and 180° turns.

5.6 Summary

In conclusion, a large amount of theoretical work has been carried out to determine how chains can be folded and unfolded without self-intersection. Considerably more publications concern recovering a straight chain from a folded state than determining exactly how many different states a straight chain can attain through being folded.

In terms of the system presented in this work, a formula for calculating how many states a chain of arbitrary length can attain without self-intersection remains to be discovered, but the number of states for small examples can be derived by both removing candidates which are proven to always self-intersect and by inspection. Using only 90° or 180° turns, all convex and monotone polygons can be filled in using the method presented in this work. The level of accuracy when shape-filling depends on both the geometry of the shape to be approximated and the relative size of the shape and the tiles. Other shapes, such as spirals and hollow shapes, can also be made. Simulations and physical experiments of some folded shapes will be presented in the following chapter.

Chapter 6

Design Series II

In the next main design iteration, inspiration for the magnet kinematics was drawn from a video by Dr. Kazuo Hosokawa at RIKEN. In the video, there are cube-shaped blocks each containing two magnets that can slide a certain amount within the cube. When the cubes are placed adjacent to each other, the magnets inside each cube are attracted to each other more than to magnets in any other cube, and so each cube can be moved about independently. When the cubes are placed in a line and a lone magnet is placed near one of the cubes' faces, the magnets within the cubes rearrange, resulting in the line of cubes being held together by magnetic forces. This concept serves as the basis for development of the research presented in this chapter.

When analysing this system, it is clear that the rearrangement of magnets is only possible because of the paths restricting their movements. If the two paths in each cube were made into one, the magnets would immediately connect together and another magnet of the same magnetic strength would not be able to separate them. On the other hand, overly restrictive paths would not allow the system state to change at all. With this in mind, this chapter contains inequalities that have been derived concerning path length and placement, which must be met in order for magnet reconfiguration to be attained.

6.1 Path Length Inequalities

Figure 6.1 depicts the generic layout for a system of tiles based on Hosokawa's cubes. All magnets are assumed to have the same magnetic moment and size.

The key distances for each part of the tile are labelled in Fig. 6.1(a): a is the total length of each path, b is the distance between the centres of the magnets when in their initial positions, and c is the distance between the tile edge and the centre of the magnets when

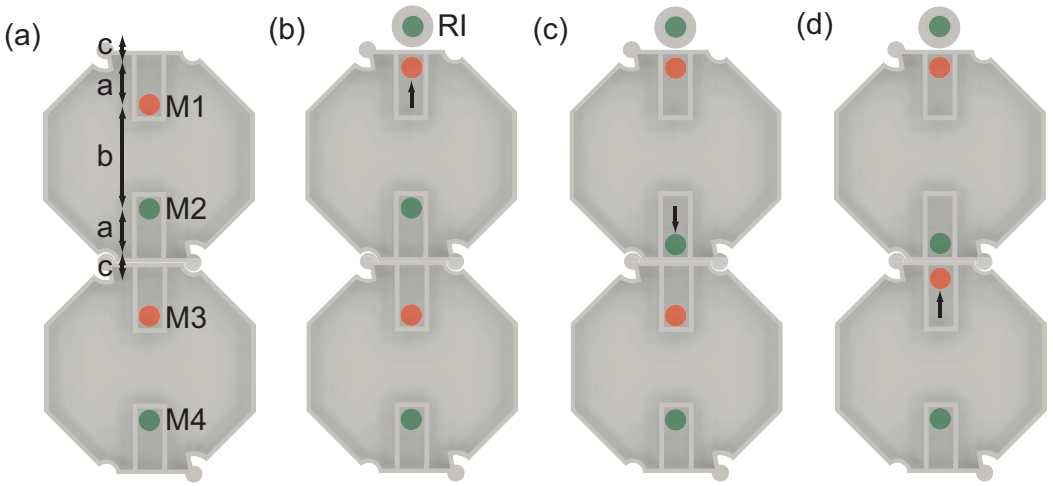

FIGURE 6.1: Overhead view of linear propagation stages for a system of two tiles. Green and red magnets indicate North and South poles facing upwards, respectively (although ordering is irrelevant provided that the poles alternate). (a) Initial locations of magnets. Intra-tile distance is shorter than inter-tile distance and so the tiles are only weakly attracted to each other. (b) Reaction initiator (RI) approaches the system until M1 is closer to RI than it is to M2, and so M1 moves towards RI. (c) M2 is now closer to M3 than it is to M1, and so M2 moves towards M3. (d) M3 is now closer to M2 than it is to M4, and so M2 moves towards M3. Intra-tile distance is now shorter than inter-tile distance and the tiles become strongly attracted to each other.

in their final positions. The tiles are designed to be rotationally symmetric in order to reduce the number of tile types required to form shapes. Inequalities derived from each stage in Figure 6.1 are as follows:

(a) Magnets in their initial locations. Intra-tile distance $= b$. Inter-tile distance $= a + 2c + a$. Thus, for the magnets to remain in their initial positions:

$$b < 2c + 2a \tag{6.1}$$

(b) RI approaches, and can potentially move all the way to the outer edge of the tile (depending on whether the RI is in a holder and the size of this holder). The RI must be able to come close enough for M1 to begin moving towards it:

$$c + a < b \tag{6.2}$$

(c) M2 is now closer to M3 than M1, and so moves towards M3:

$$2c + 2a < a + b \tag{6.3}$$

(d) M3 now moves similarly to that shown in (a), however M3 cannot come as close to the edge of the tile as the RI may be able to do:

$$2c + a < b \tag{6.4}$$

If this chain were longer in length, then the inequality in order for M4 to begin moving is identical to that in (c).

Equations 6.3 and 6.4 are then repeated up to the final tile in the chain, where the final magnet (M($2N$) for a chain of length N) does not change position.

Equations 6.1 to 6.4 can be simplified to

$$2c + a < b < 2c + 2a \tag{6.5}$$

which is the final inequality concerning path lengths that the system must follow in order for it to work successfully.

6.2 Locations of Path Start and End Points

Possible values for the lengths of paths have now been determined, but rules concerning the initial and final locations of the magnets must still be derived.

Since $2c + 2a + b$ is equal to the total length of the tile, from Eq. 6.1 it can be deduced that b must be less than half of the total tile length. The tiles in Figure 6.2 are split into three sections with dashed lines, such that the centre section is half of the total tile length. Thus, the initial positions of the magnets must be on the dashed lines or inside the centre section. The total path length a can be split into two parts: $a = s + e$. s denotes the amount by which the initial magnets are inside the centre section, and e denotes the length of path outside of the centre section. s can be equal to zero, which would cause all magnets to initially be equidistant. We therefore know that:

$$0 \leq s \tag{6.6}$$

$$e < \frac{d}{2}. \tag{6.7}$$

More detailed information about the timing of when each magnet begins movement can be derived using s and e. Figure 6.2 shows the identical process to Figure 6.1 but in

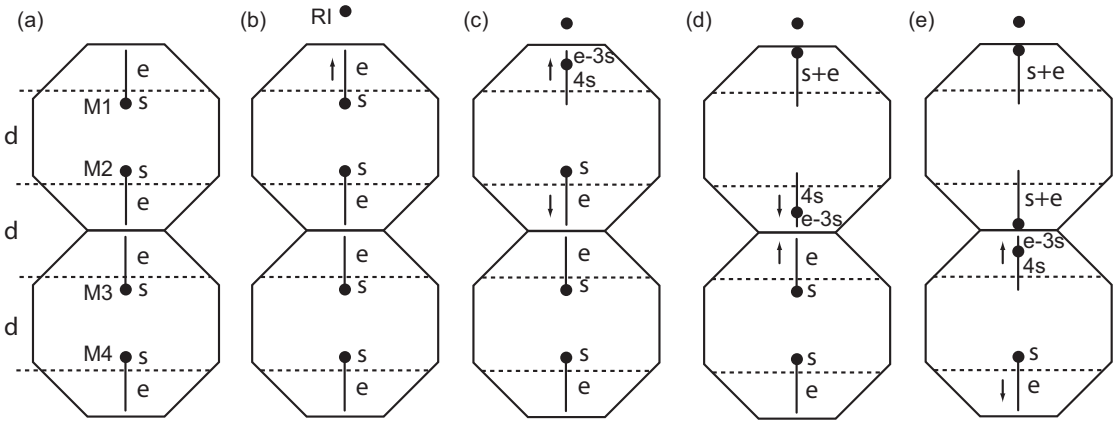

FIGURE 6.2: Stages of attraction and propagation with respect to s and e. (a) Magnets in initial positions. Dashed line indicates the length of s: if $s = 0$, magnets' initial positions would be on the dashed lines and all magnets would be equidistant. (b) M1 is attracted to RI. (c) M1 has travelled far enough away from M2 that M2 is now more attracted to M3 than M1. (d) M2 has travelled close enough towards M3 that M3 is now more attracted to M2 than M4. (e) M4 would begin moving towards M5 at this stage for chains longer than two tiles in length.

more detail. Magnets inside tiles have not begun to move in (a) and (b). In (b), the distance between M2 and M1 is $d - 2s$ while the distance between M2 and M3 is $d + 2s$. In (c), M1 has moved sufficiently towards RI such that M2 is equidistant to M1 and M3. This means that M1 must move a distance of $4s$ for M3 to begin moving. M2 and M3 must also move a distance of $4s$ before M3 and M4 begin moving, respectively. If each magnet must be able to move a distance of $4s$, we can see that

$$4s \leq s + e. \tag{6.8}$$

Equations 6.6-6.8 can be rearranged to form

$$0 \leq s < \frac{e}{3} \tag{6.9}$$

$$e < \frac{d}{2}. \tag{6.10}$$

6.3 System Tuning

In order to produce a strong inter-tile attraction after propagation has reached the end of the chain, e is chosen to be as large as possible. However, the value of s can be altered in order to vary the system's behaviour.

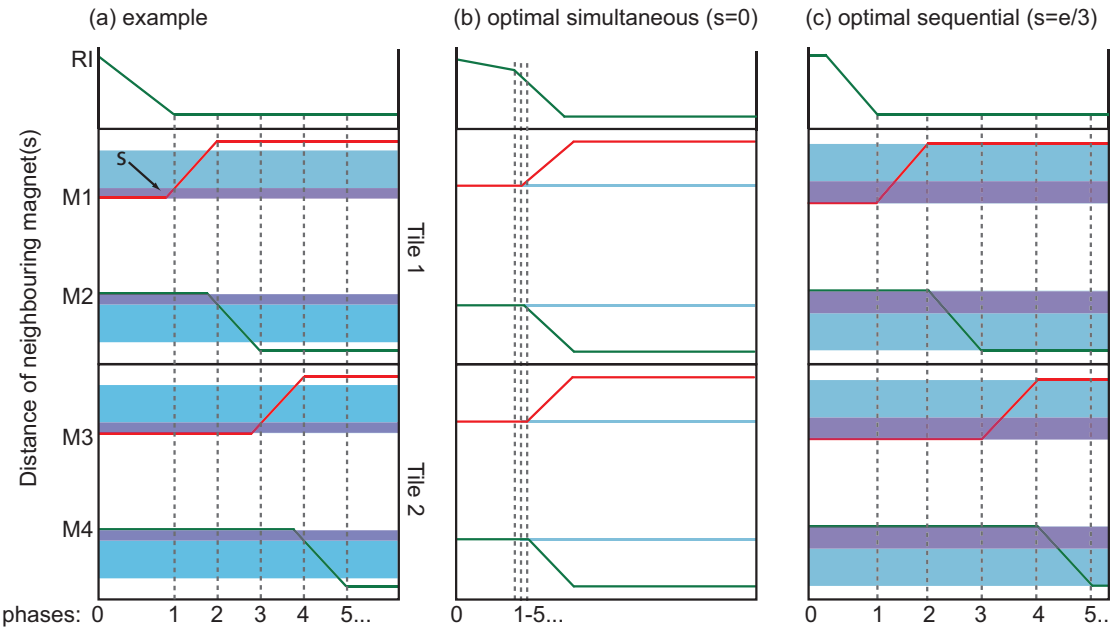

FIGURE 6.3: Transition diagrams for three different values of s. Red and green lines mark magnet trajectories, purple regions indicate the length of s, and blue regions indicate the distance the magnet must travel in order for propagation to be successful. (a) Example value of s. The next magnet will begin moving while the previous magnet is still travelling along its path. (b) $s = 0$. Magnets only need to move an infinitesimal amount to trigger propagation. (c) $s = \frac{e}{3}$. The next magnet will only begin moving once the previous magnet has travelled the full length of its path.

From earlier figures it can be seen that more than two magnets can be moving simultaneously during the magnetic propagation process. As only two magnets are required to produce a magnetic 'bonding' between blocks, this can be seen as an overlap of interaction between pairs of magnets. An example value of s and the resulting overlapping interactions can be seen in Figure 6.3(a). The amount of overlap can be varied by changing the length of s. Two key examples highlight the usefulness of this property:

1. $s = 0$ seen in Figure 6.3(b). All magnets begin equidistant to each other and so any movement of a magnet will cause a cascade effect through the system. This would be a case of optimum simultaneous assembly as all magnets move at virtually the same time.

2. $s = e/3$ seen in Figure 6.3(c). In this situation a magnet will have to travel the full length of its path before the next magnet will be equidistant to the magnets on each side of it. If an infinitesimally small length ϵ is added to e then the next magnet will be able to begin moving. This would be a case of optimum sequential assembly as only one magnet will be moving at any given time.

6.4 Chosen s Length

The final length chosen for s is $0.3mm$, equivalent to approximately $\frac{3}{50}$ of the total path length. At first glance this appears to be a negligible amount, but when considering the relative forces between magnets this produces a significant energetic difference.

For magnets with the same magnetic moment magnitude m, the magnetic potential energy between two magnets M_i and M_j is

$$U_{ij} = -\sigma_{ij}\frac{\mu_0}{4\pi}\frac{m^2}{r_{ij}^3}. \tag{6.11}$$

σ_{ij} is equal to 1 if the magnets are attracted to each other and -1 if they repel each other, $\mu_0 = 4\pi \times 10^{-7} Hm^{-1}$ is the permeability of free space, and r_{ij} is the position vector separating them.

The resultant force is

$$F_{ij} = -\frac{dU_{ij}}{dr} = -\sigma_{ij}\frac{3\mu_0}{4\pi}\frac{m^2}{r_{ij}^4}. \tag{6.12}$$

If s is chosen to be zero, then clearly the inter-tile and intra-tile magnetic forces in the chain will be equal. By increasing s to $0.3mm$, the inter-tile force increases by approximately 17.73%, the intra-tile force decreases by approximately 14.52%, and the ratio between inter- and intra-tile forces becomes approximately $7:5$. Although larger values of s are theoretically possible given the value of e, similarly to Chapter 4 there are issues with magnetic forces being too close in strength to allow propagation if s is chosen to be near the maximum possible value.

6.5 Curved Paths

Curved paths are necessary to produce folding motions in the chain. The final position for the magnets in curved paths must be sufficiently past the hinge centre in order to produce torque. Location of the final point and associating distances are shown in Figure 6.4(a). As the magnets used in the system have diameter $3mm$, a distance of $1.5mm$ ensures that the entire magnet can pass the hinge centre. The final point is also chosen to be as close to the bottom edge of the tile as possible in order for intra-tile strength to be strongest. Both of these criteria cause the magnet's final position to be fixed in both x and y axes.

Another important location in the curved path is marked in Figure 6.4(b). It is the closest distance between the magnet that has started moving down its curved path, and

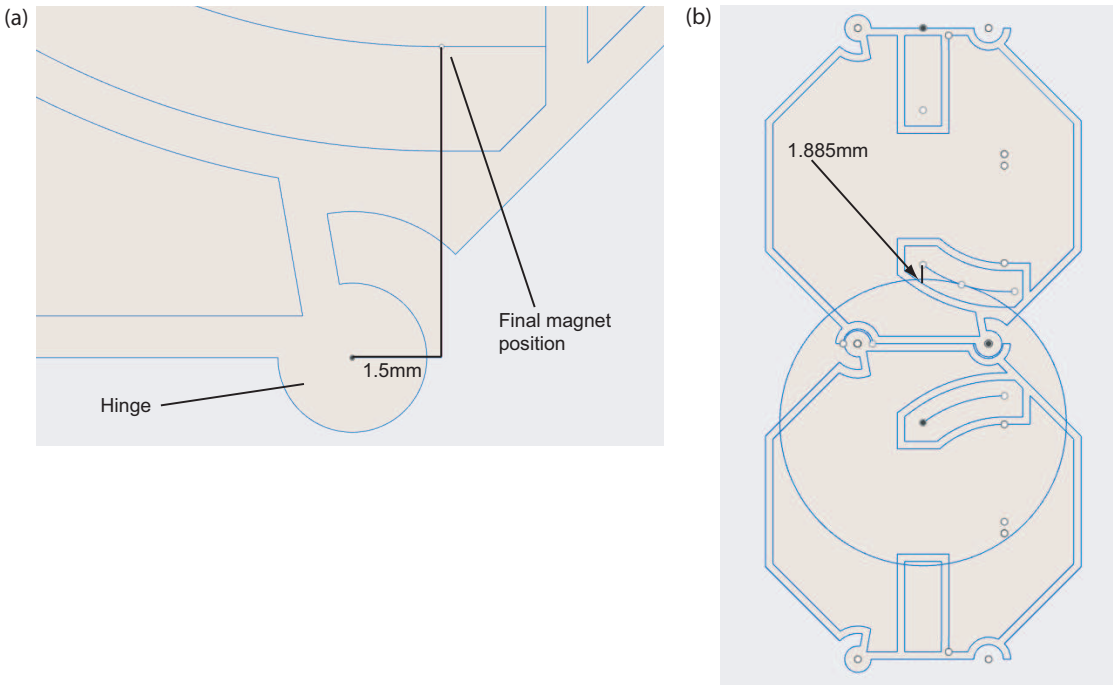

FIGURE 6.4: Considerations during the design of curved paths. (a) Location of final positions for magnets in curved paths. (b) Overhead view of two tiles with curved paths. Circle is centred at the initial position of the third magnet in the chain, showing the point on the path of the second magnet where they will be closest in distance. The third magnet must be able to begin moving before the second magnet reaches this point in order for propagation to be possible.

the next magnet in the chain (also located in a curved path) while it is still in its initial position. Due to the curved nature of the path, the next magnet in the chain must have begun moving before the previous magnet has reached this point in order for propagation to continue. Thus, the distance between the magnet's initial position and this point is the equivalent of the length e in the curved path. In the final tile design, the distance is found to be $1.885mm$, and thus $s = 0.3mm$ is suitable for both straight and curved paths. This allows all of the magnet's initial positions to be identical, regardless of path type.

The full design for the curved path is as follows: the magnet starts in their initial positions, once released it moves directly towards the next magnet for a distance of $0.3mm$ (equivalent to s), and then travels along the arc of a circle that connects to the magnet's final position point (see Figure 6.5). The circle arc is drawn such that it is tangent to a line drawn horizontal to the final position point. This ensures that the angle between two curved paths decreases monotonically but at a gradually slower rate, until the final angle between two magnets on the paths is zero. In theory, the paths that cause folding could be straight and at an angle to each other, or even asymmetric with a straight path in one tile and an angled path in the other. However, although designs following these principles worked in simulation, friction in physical experiments

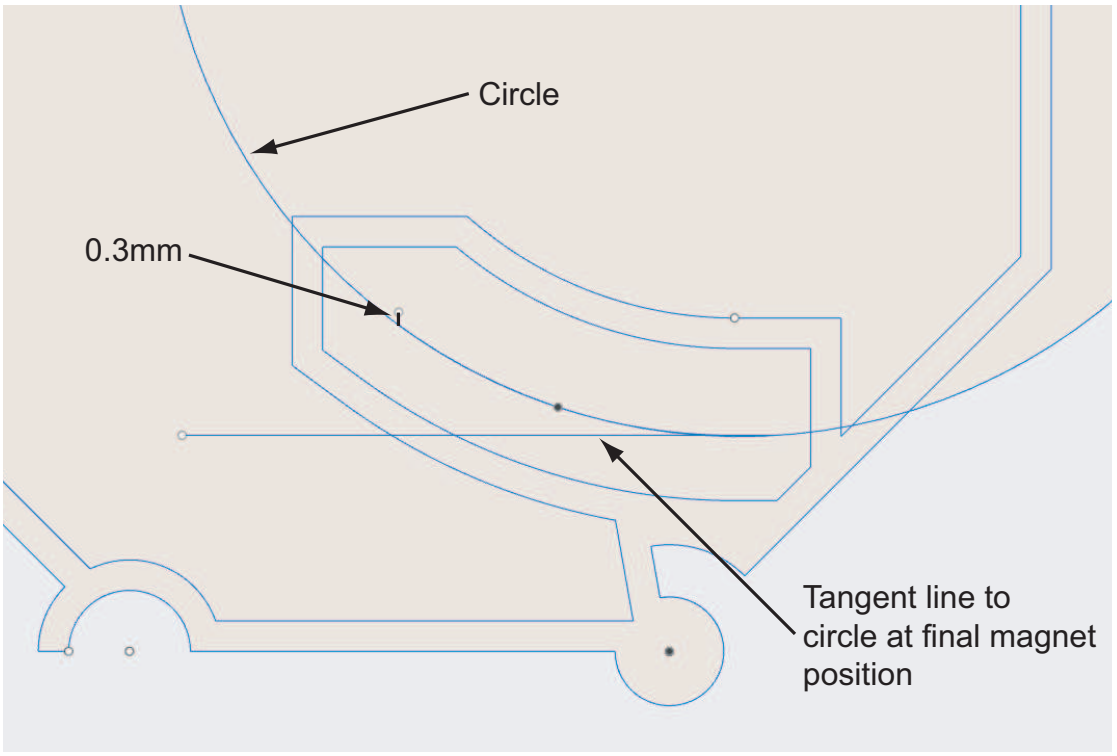

FIGURE 6.5: Schematic of the final curved path design.

between the magnets and tile walls prevented magnets from moving smoothly or at all (see Appendix A). Designs using curved paths of any type performed significantly better than those with paths containing straight sections.

The final schematic for the stages of attraction and propagation for this set of s and e values are shown in Figure 6.6. Magnetic flux lines in (b) show how the RI is attracted to M1. If the RI approaches from the chain's side, the RI can be trapped by the attractive field of other magnets and potentially inhibit propagation down the chain. However, the RI can be attracted from various different angles and still successfully trigger the movement of M1.

6.6 Summary

This discovery brings about a relatively unexplored area in the field of self-assembling systems. Previous works, both theoretical and experimental, have produced systems that correspond to the optimum simultaneous assembly paradigm or the optimum sequential assembly paradigm, either through assumption or by design. In [5], the shape memory polymers used at each hinge are varied to produce a simultaneous system and a sequential system, but nothing in-between is explored. The calculations here give rise to the idea

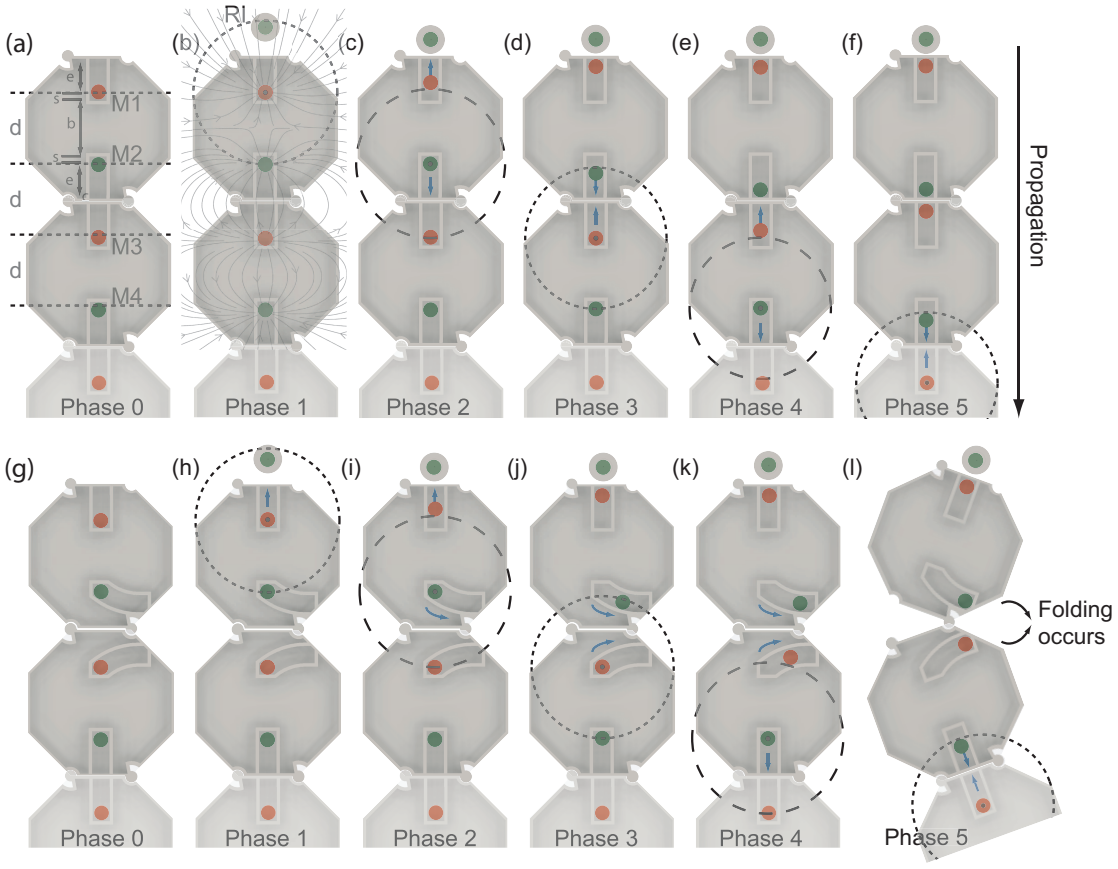

FIGURE 6.6: Stages of attraction and propagation for the final path designs. Dashed circles centred at magnets signal that the distances from adjacent magnets are equal. Radius of circles with small dashes is $d-2s$; radius of circles with large dashes is $d+2s$. (a)-(f) Stages for linear (non-folding) propgation. Magnetic flux lines in (b) indicate how the RI can be attracted to magnets in the chain and the direction in which it must approach in order for movement of M1 to be triggered. (g)-(l) Stages for folding propagation.

that a system's behaviour can be easily tuned, where the point at which the next module is initiated can be a deterministic outcome of the geometry of the system.

Chapter 7

Results

The previous chapters have included some derivations of theoretical results under optimal conditions. It is thus important to prove that these results can be applied to real systems and produce successful outcomes, even in the presence of variables such as mass and friction that were not included in derivations. This chapter will provide descriptions of results from simulations and experiments, with technical details of the simulation environment located in Appendix A.

7.1 Final Tile Designs

Figure 7.1 depicts the final design of the tiles used in the results presented in this chapter, described as SS, RS, RR, and SR. The external geometry of each tile and the initial positions of all magnets are identical in each tile and rotationally symmetrical. This allows for tiles to be rotated 180° to produce tiles SL, LL, and LS (SS is rotationally symmetrical). The tile LR (equivalently RL) is also a valid path configuration and would produce designs containing diagonal lines, but this tile type was not needed in the system as current designs are produced using rows of tiles that are either parallel or orthogonal to each other. The hinges are designed (initial design carried out by Valentin Besnard, updates made by the author) such that the tiles in a chain remain aligned during folding, but at no point are the tiles permanently connected together. This is to allow the possibility in the future for chains to also be self-assembled from individual tiles.

The external shape of the tiles without considering the hinge structures is a regular octagon. This means that the external angles of the walls are 45° and so, when a folding action is completed, a 90° angle is produced between the pre-fold section of the chain

and the post-fold section of the chain. A diamond could have been chosen as the base shape of the tile instead and the same result would have been produced, but an octagon has the additional attribute that there are no parts of the tile that could touch each other during folding and thus the chances of accidental collision are reduced.

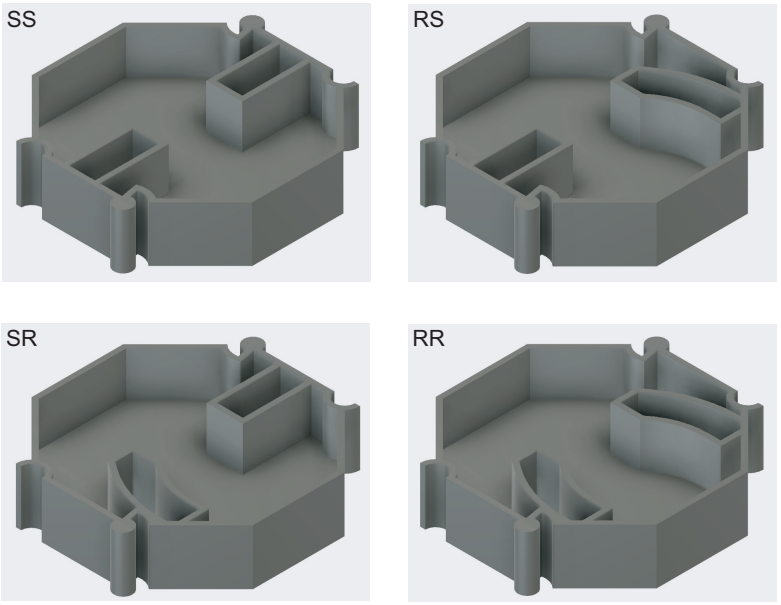

FIGURE 7.1: Final line-up of tiles used in results. Clockwise from top-left: two straight paths (SS), curved path followed by straight path (RS, equivalently SL), two curved paths (RR, equivalently LL), straight path followed by curved path (SR, equivalently LS).

7.2 Simulations

The maximum length of chains in physical experiments was limited due to the size of the available environment. Small simulations were carried out to test the feasibility of path designs during the development process, and subsequently the same environment could then be used to test the feasibility of tile configurations that couldn't be tested in reality. Simulations of larger experiments are presented below. All simulations were made using Blender Game Engine and the Bullet physics library- more details and images are available in Appendix B. Figure 7.2 shows a 107-tile square being made with 180° turns formed from LL and RR tiles. It is clear to imagine that many different shapes can be made by changing the lengths of the straight sections of the chain. Meanwhile, Figure 7.3 shows a 82-tile square with looser turns formed without using LL and RR tiles, demonstrating that configurations containing areas of higher and lower tile density are also possible. Finally, Figure 7.4 shows a 171-tile 'key' shape being made using 180° and 90° turns, identical to the shape proposed in Figure 5.6. This demonstrates the ability to make functional structures using this system.

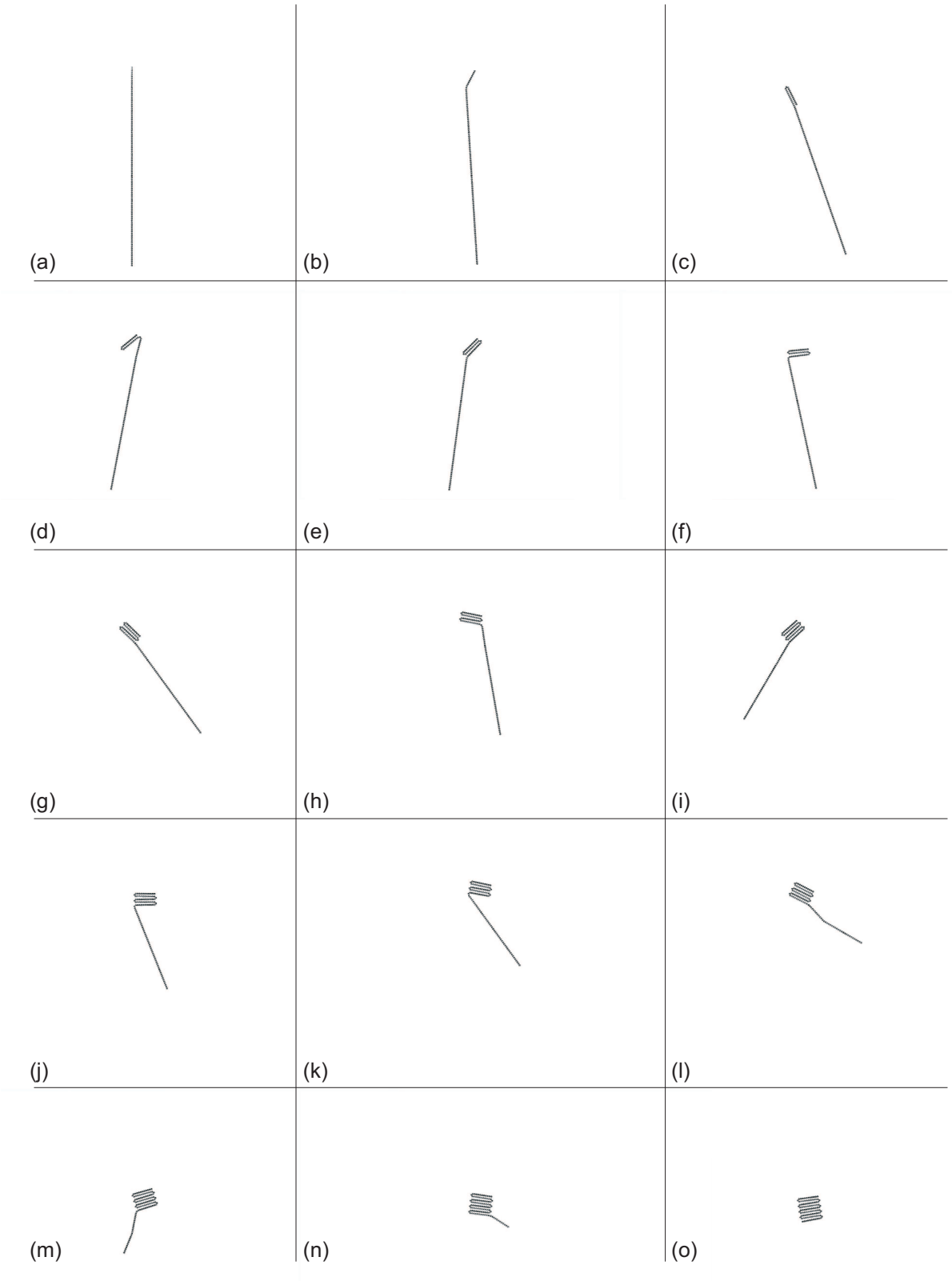

FIGURE 7.2: Simulation stages for a square composed of 107 tiles. The configuration is composed of four tile types.

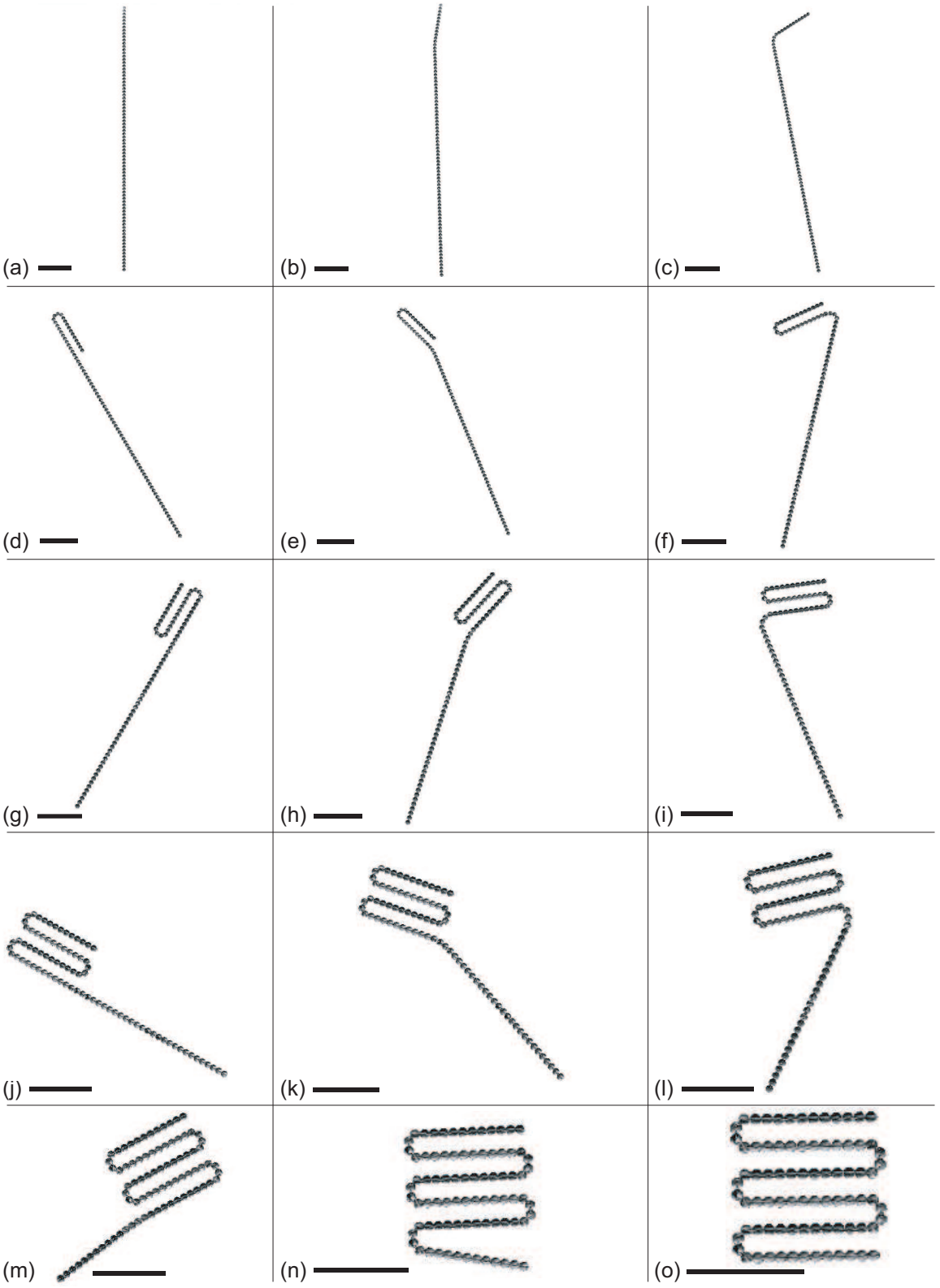

FIGURE 7.3: Simulation stages for a square composed of 82 tiles. The configuration is composed of three tile types and thus the turns are looser than in the previous figure. Scale bar is set as the length of 10 tiles.

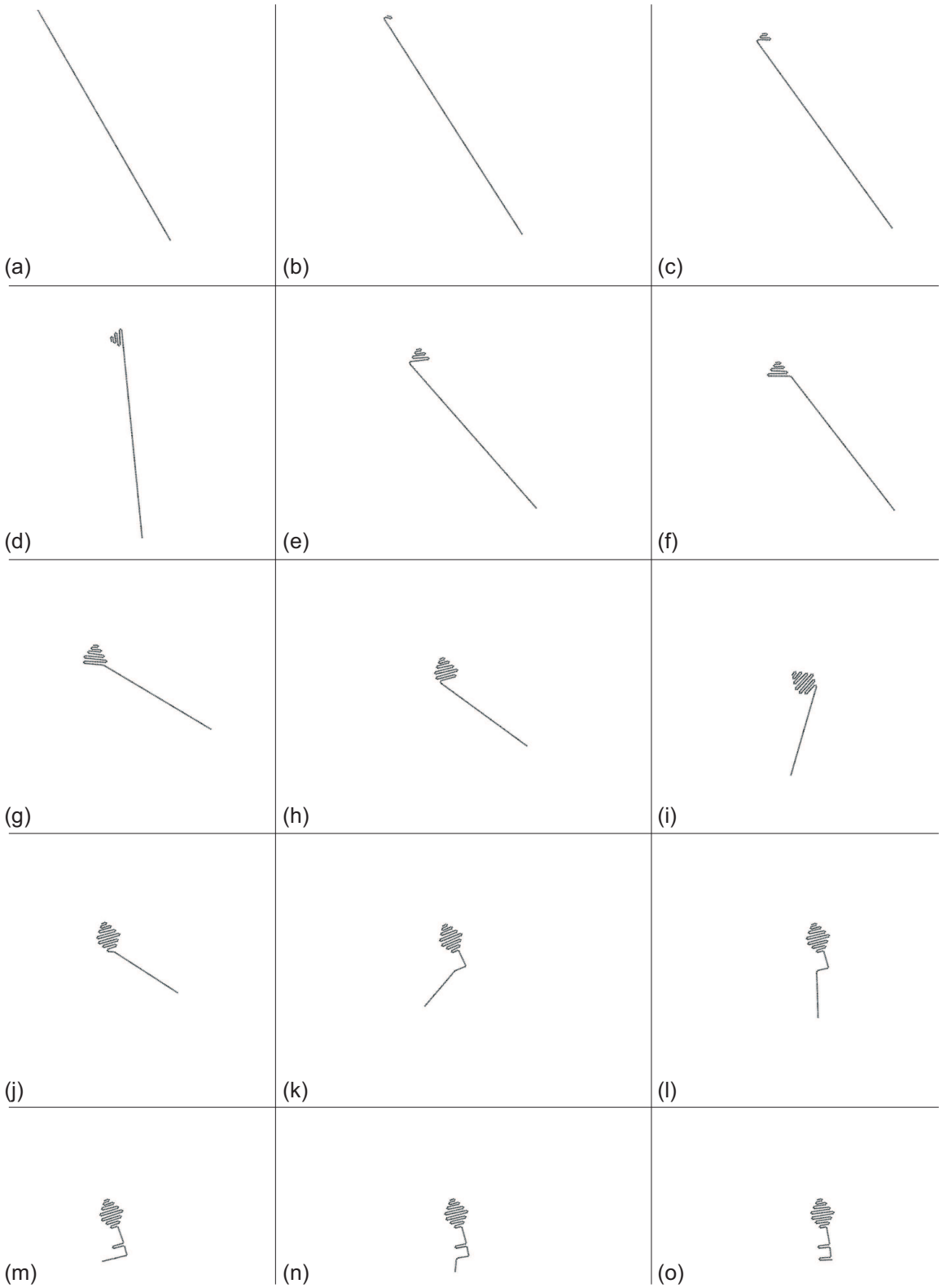

FIGURE 7.4: Simulations stages of a key shape composed of 171 tiles. This design incorporates a 90° turn.

7.2.1 Potential Energy Graphs from Simulations

The distances between adjacent magnets can be read from the simulation software and then used to calculate the potential energy at every time step during the simulation. It can be seen in Figure 7.5 that the potential energy of the system decreases approximately linearly until the final configuration is reached, which corresponds to one of the proposed optimisation criteria presented in the previous chapter. Small spikes in the energy graph are due to minor errors during simulation.

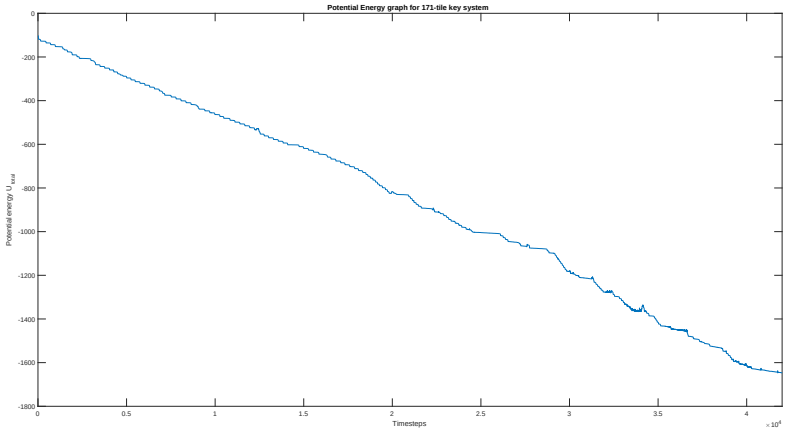

FIGURE 7.5: Graph of magnetic potential energy decay for the key simulation, calculated from over 16 million data points taken throughout the simulation.

7.3 Experiments

$3cm \times 3cm \times 7.5mm$ tiles are designed using AutoDesk Fusion 360 [83] and 3D-printed with a Stratasys Objet500 Connex3^{TM}, using plastic with a 'glossy' finish to prevent absorption of water during experiments. The tiles are placed in a container with a small (approximately $5mm$ depth) amount of water. Water reduces the level of friction between the underside of the tile and the container, but if too much water is used there can be difficulties with water resistance acting upon the tiles during folding, and it is more difficult to ensure that the tiles remain in the same plane during actuation. The tiles can move about on the air-water interface and naturally attract each other in the correct orientation to form a chain due to magnetic forces, but cannot spontaneously actuate because the intra-tile forces are stronger than the inter-tile forces. Another magnet (the RI) must still be deployed in order for the chain to be actuated.

Figure 7.6 shows stages from two experiments using the final tile design: linear propagation followed by a 90° turn, and two consecutive 90° turns to form a 180° turn. The magnets used are $3\theta mm \times 5mm$ nickel-plated, neodymium disc magnets purchased from Supermagnete [84], with weight $0.625g$ each and strength of approximately $5N$.

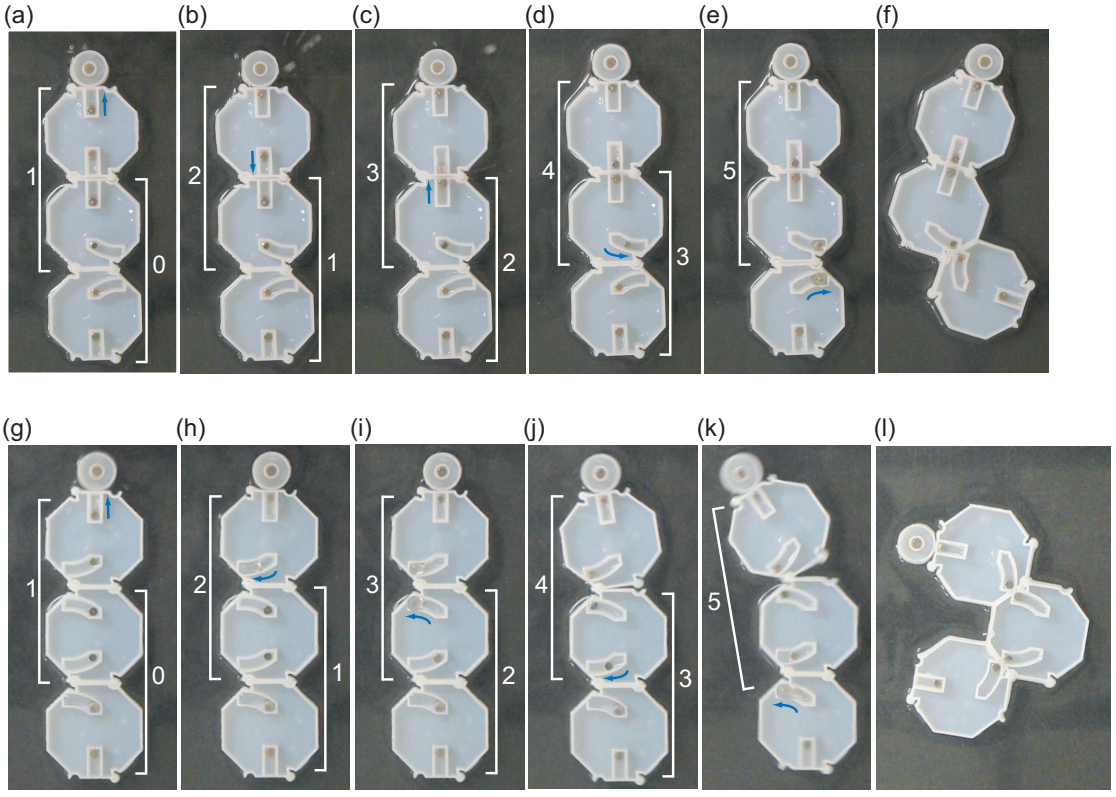

FIGURE 7.6: Examples of chains folding while floating on water. Brackets and numbers indicate associated phases for each pair of tiles. (a)-(f) Three tiles, comprising linear propagation between tiles followed by a 90° turn. (g)-(l) Three tiles comprising two consecutive 90° turns resulting in a 180° turn.

The magnets are coated in silicon oil (Johnson & Johnson^{TM}) prior to being inserted into tile paths. Water is then added inside the paths level to tile walls. The container for the system has height $7cm$ and diameter $40cm$. Experiments were filmed using a Casio^{TM}EX-FH20 camera.

The brackets and numbers in the figure above indicate the phases for each pair of tiles corresponding to those presented in Figures 6.3 and 6.6, and it can be seen that the magnet kinematics in experiments match those predicted. As well as the experiments pictured, two more types of tests were carried out with three tiles (two consecutive cases of linear propagation, and a 90° turn followed by one linear propagation) to complete the set of all possible configurations for three tiles. Each test was carried out 5 times with a 100% success rate: magnetic propagation successfully reached the end of the chain, and the final tile configuration matched the predicted tile configuration.

An unexpected finding from these experiments was the ability to easily 'reset' the tiles after an experiment had been carried out. After an experiment has been completed, the entire configuration can be easily lifted out of the container as one piece due to the strong magnetic attraction between tiles. The tiles are then separated by hand. Once

the tiles are separated from each other by a certain distance, the magnetic attraction between the pairs of magnets within each tile dominates and the magnets move back towards their initial positions. This means that the tiles automatically reset themselves and become ready for re-actuation, a departure from many other self-assembly systems which require significant resetting procedures or may only be actuatable once.

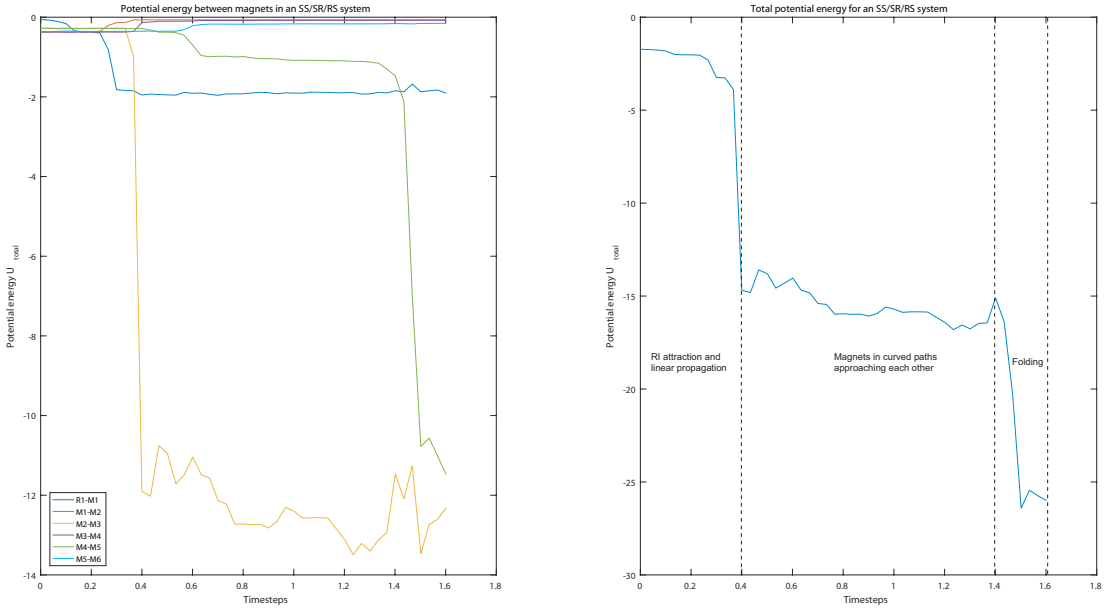

FIGURE 7.7: Potential energy for (left) each pair of adjacent magnets and (right) total potential energy of a chain composed of linear propagation by a 90° turn. Dashed line indicate different phases of actuation.

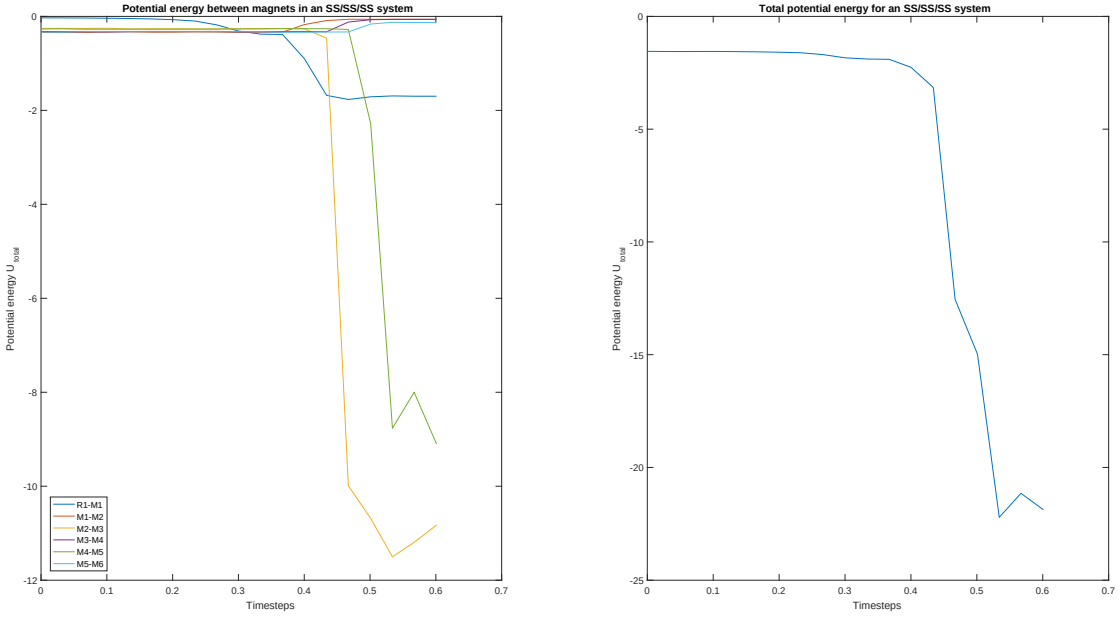

FIGURE 7.8: Potential energy for (left) each pair of adjacent magnets and (right) total potential energy of a chain composed of two consecutive linear propagations.

7.3.1 Potential Energy Graphs from Experiments

The positions of each magnet during an experiment were recorded using motion tracking software (Tracker). The data is then fed into a Matlab script which calculates the magnetic potential energy between each magnet over time. The values can be processed to find the change in total magnetic potential energy in the system throughout actuation. Sample potential energy graphs corresponding to (a)-(f) and (g)-(l) in Figure 7.6 can be seen in Figures 7.7 and 7.8, respectively. Spikes in the graph can be explained by the kinetic energy of magnets 'bouncing' when they reach the end of their paths and when tile walls collide with each other at the end of a folding process, as well as general noise produced from manually tracking the data.

7.3.2 Random Chain Configurations

A feature noted during experimentation was that, although the paths were designed to be paired in straight-straight or curved-curved configuration, linear propagation is still successful if a straight path is matched with a curved path. In this sense, the tile sequence SL-SR-SL would produce the same outcome as the sequence SS-SS-SS. Meanwhile, pairing a path that curves to the left and a path that curves to the right (e.g. SR-LS or LL-RS) inhibits propagation to continue along the chain. This brings about interesting questions regarding chains that are formed from random configurations of tiles and the associated probabilities of each configuration actuating successfully. A table of all path pairings and their outcomes are displayed in Table 7.1.

Path Configuration	**Outcome**
SS	Linear Propagation
SL	Linear Propagation
SR	Linear Propagation
LS	Linear Propagation
LL	90° Fold
LR	Propagation Inhibited
RS	Linear Propagation
RL	Propagation Inhibited
RR	90° Fold

TABLE 7.1: Table listing all possible pairs of straight, left-curved and right-curved paths, and respective outcomes when the pairs are actuated.

It can be seen that, if two tiles are randomly placed next to each other, there is a $\frac{5}{9}$ probability that the outcome will be that of linear propagation, $\frac{1}{9}$ probability that a folding motion will be produced to the left, $\frac{1}{9}$ probability that a folding motion will be produced to the right, and $\frac{2}{9}$ probability that propagation will be inhibited. If a chain

of N tiles is formed from a random selection of tiles then it is reasonable to suggest that any permutation of paths is equally possible, but the outcome of these chains will not have equal probability. The probability that propagation will reach the end of the chain successfully (without taking potential chain self-intersection into account) is $(\frac{7}{9})^{N-1}$. It is significantly more likely that there will be sections of consecutive linear propagation rather than sections of consecutive turns- something that aligns well with the current technique for producing shapes using the chain.

7.4 Summary

Many self-assembling systems in the literature are purely theoretical or, if there is some sort of physical representation of the work, it is greatly simplified from the system proposed in the methods. In this work, the theory has been clearly represented in a physical system that matches well in terms of predicted and realised output. An additional feature of the system was also recognised through experimentation, that of the magnets inside each tile resetting to their original positions once the tiles have manually separated. This will be very useful when the tiles are scaled down in size and manipulating the magnets becomes difficult.

The simulations have also proven to successfully replicate the real-life results of the system. The simulation environment can thus be used to not only as a test bed for prototype tile and path designs, but also as a method of demonstrating the potential of the system when a much larger amount of tiles is employed. Currently, work is been carried out by Etienne Perroux to optimise the Python scripts used in the system so that much larger simulations (in the order of thousands of tiles) can be carried out.

Chapter 8

Conclusion and Future Work

Figure 8.1 shows a schematic of the final design with labelled phases of actuation. In this work, a deterministic, distributed, bottom-up self-assembly system has been developed, which can form two-dimensional shapes using permanent magnets as its only mechanism. In Chapter 3, a list of design criteria was developed in order to inform the design process, and it is the belief of the author that this system has met all of the criteria. The idea of applying the conditions of Anfinsen's dogma to the system was also presented within this list, and the conditions were met in the following ways:

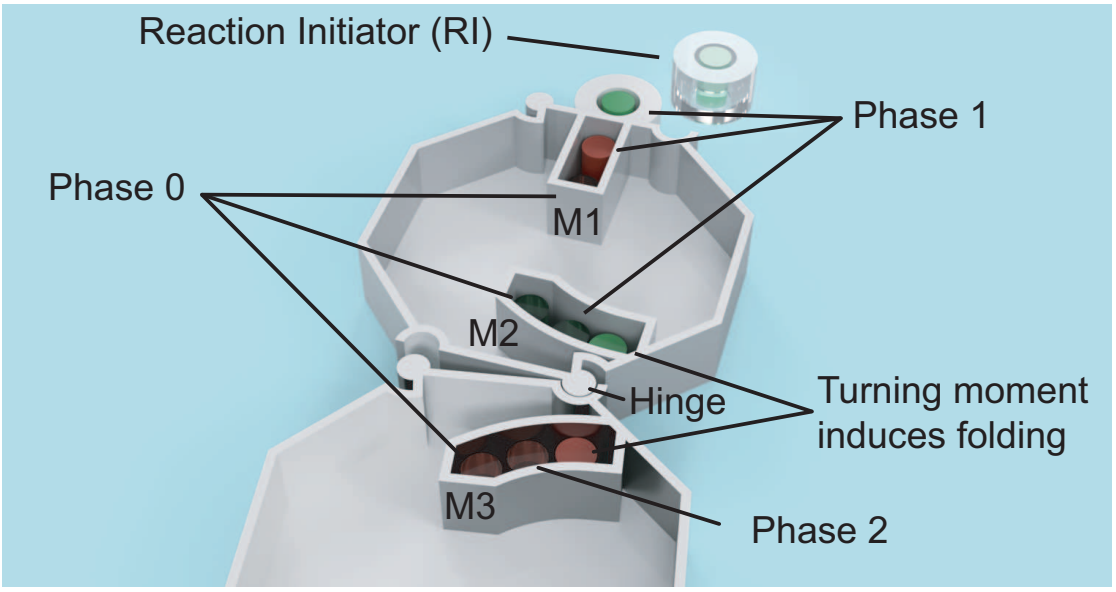

FIGURE 8.1: A rendering of the final design, with translucent and opaque magnets showing different stages of the actuation process.

1. Uniqueness: a chain of tiles will reliably reach the configuration determined by the ordering of paths within the tiles.

2. Stability: once magnets reach the end of their paths, it is close enough to the magnet in the adjacent tile such that no other magnets will subsequently be able to separate them. They are also unable to separate due to perturbations caused by folding motions later on in the chain.

3. Kinetical Accessibility: the final chain configurations are composed completely of 90° and 180° turns, and any chains that self-intersect are avoided.

After deriving these criteria, an analysis of the most recent work on the subject was carried out and the main issue was highlighted- self-intersection of the chain greatly reducing the conformational space of the system. A review of work on collision theory and algorithms was then presented to clearly illustrate the knowledge in this area. A system capable of avoiding the self-intersection issue was then presented. This required careful calculations to discern the properties of paths which hold the magnets that control the system in position.

The inequalities derived concerning the size and placement of paths inside the tiles are non-specific to this specific work, and so could be transferred directly to future publications. The theories have been realised successfully in physical experiments, which is remarkable in the sense that most works on self-assembly in the literature based on enthalpic principles have not yet been successfully translated to real life. Finally, simulations of longer systems indicate the ability to produce larger, more detailed shapes with increased functionality.

It is clear that this area of research is still in its nascence and there exists countless avenues for further development. There also some applications which are clearly foreseeable for this type of system. The final chapter in this work will present some examples of each.

8.1 Applications

There are some foreseeable applications for the system, with and without the developments described in the previous section. A non-exhaustive list is provided below:

- Metamaterials and metastructures- these are materials and structures composed of elements that have also been artificially engineered, allowing the final product to exhibit properties that cannot be found (or are found only with significantly reduced capabilities) in nature. One could envision micro-scale versions of this system being employed to produce metamaterials or metastructures with high levels of reconfigurability and re-usability.

- Microscale manufacturing and fabrication- self-assembly is a key technique used in micro-manufacturing and micromachining, as it becomes extremely difficult to produce detailed, three-dimensional structures at the micro-metre scale [85]. Small-scale versions of this system could produce complex structures with minimal interference or, alternatively, could be used as a type of scaffold for other materials. The scaffold can be used to dynamically configure a material into its intended shape, and then can be removed from the configuration environment with a magnet.
- Entertainment- users of the system can plan their own structures, build the chain and actuate it to see the results. Similar products exist in the market already, such as the 'Snaak' toy which was successfully crowd-funded in 2014 [86].
- School-age education- students can learn about magnetic attraction and repulsion through experimenting with the self-assembly of different structures.
- Higher-level education and research - the system was primarily inspired by protein folding and biologists attempts to understand how the minimisation of free energy determines the folding and native state of a protein strand. Now, this system could be used as a visualisation tool for those working on the protein folding problem.

8.2 Avenues of Further Research

This section will discuss some (but certainly not all) of the potential areas of development for this system.

8.2.1 Scaling the System

Any environment for the system at its current size must be able to contain not only the chain in its initial configuration, but also the chain as it folds in various different directions. This makes any system containing large numbers of tiles prohibitively difficult to set up and actuate. However, this system has been designed specifically to scale well into smaller dimensions.

Firstly, it has been well known that magnets can be made at much smaller sizes than those used in this work. Magnets of less than $1mm^3$ are commercially available, and magnets comprising a single atom have recently been produced [87], although their shelf life is currently only a few hours. If the tiles become so small that the attractive forces of the magnets are no longer strong enough to attract each other, the magnetic strength can be increased by increasing the magnet height. This is because the magnetic moment

will scale proportionally to the magnet volume. However, care must be taken that the centre of mass for the magnets remains lower than the tile wall height to prevent magnets from escaping their paths, and that the mass of the magnets does not inhibit movement.

The reason that mass will affect magnetic movement is because an increased mass will increase the friction between the magnet and the tile base. Friction is something that has been largely ignored during this work, in part because it would be highly complex to model due to the addition of water and oil as lubricants. Clearly, the force acting on a magnet must overcome the static friction between the magnet and the base before it can start moving [88], and will likely affect the possible values of s during path design. Friction at very small scales is exceptionally complicated and there is no definitive theory for how it should be approximated, and so a version of this system at the μm-scale should ideally take this into account during modelling.

Lastly, this system has significant benefits over many mechanical systems due to the scaling effects of magnetic force. Ma et al. [52] analyse the scaling properties of forces in a magnetically-actuated system and confirm that magnetic forces scale favourably: torque between a pair of magnets scales in inverse proportion to the 3^{rd} order of distance r between them, while other forces such as drag force and hinge stiffness are inversely proportional to the same or higher orders of r, meaning that, as r decreases, magnetic torque will dominate over other forces that could impede motion.

It was stated at the end of Chapter 2 that mechanical self-assembling systems can achieve complex configurations but have difficulty at small scales, while chemical self-assembling systems are possible at small scales but generally can only achieve homogeneous configurations. Although it has not yet been definitively proven, it is believed that this system has the power to achieve the best from both of these properties- one that can comprise large numbers of very small modules, that are then actuatable into complex, heterogeneous, and even functional shapes.

8.2.2 Optimising Potential Energy Decay

As discussed in Chapter 3, once it is initiated the magnetic potential energy of the system continually decreases until it reaches its final state at an energetic minimum. The potential energy is calculated using

$$U_{total} := \sum_{i<j} U_{ij} \tag{8.1}$$

where U_{ij} is derived in Eq. 7.1. It is important that the potential energy decreases monotonically such that the system does not plateau and the magnets cease motion. This brings about various questions in terms of how the potential energy decay could be optimised.

One potential criteria for optimisation is to linearise the energy decay. Consider a system comprising two magnets in curved paths that are released simultaneously. They then move at the same velocity until they reach their respective final positions. Thus, the equation for paths which produces linear magnetic potential energy decay is

$$f(x) = \frac{1}{2\sqrt[3]{qx + r}} \tag{8.2}$$

where q and r are used to fit the curve to the magnet's initial and final positions. For non-folding paths, the path could be reflected such that the path returns to the tile centre.

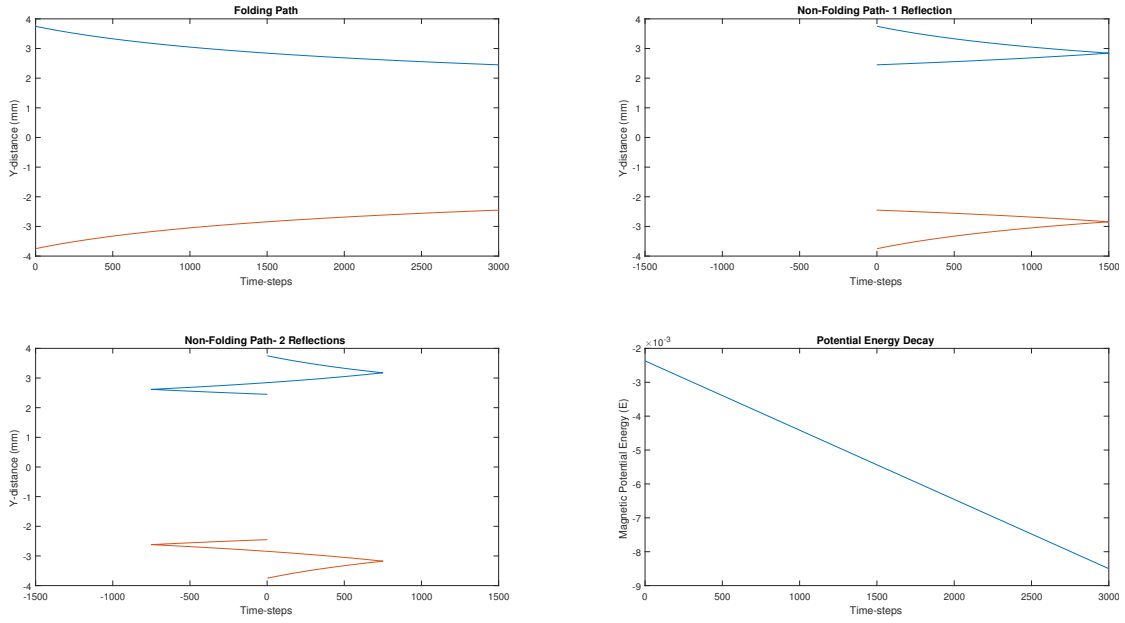

FIGURE 8.2: Paths for a pair of magnets with linear potential energy decay. Clockwise from top-left: Optimal curved paths. Non-folding paths reflected once in order for the magnets to finish at the centre of the tiles. Plot of potential energy decay between the magnets at each time step. Non-folding paths reflected twice in order for the tile mass to be spread more evenly.

Although the paths in Figure 8.2 are optimised in this specific case, it is difficult to scale this process for different or larger systems. Firstly, as both magnets must be released at the same time, it is a simplified version of specifically an $s = 0$ system. This brings about the realisation that each value of s used to define the initial magnet position will have a different optimal path in terms of its potential energy decay. Secondly, Eq. 8.2

assumes that the magnets move at a constant speed along the path length, whereas this is highly unlikely in real life.

In response to this issue, a proposed alternative criteria for optimisation is to make the magnets reach their final positions in the shortest possible time. This is closely related to the famous Brachistochrone problem, first proposed by Johann Bernoulli in 1696: given two points A and B in a uniform gravitational field, where B is lower than but not located directly underneath A, what is the shape of the curve starting at A which reaches B in the shortest possible time? The solution for this problem is a inverted cycloid whose arc dips below the position of B due to the uniform gravitational field specified by the question. It is clear that this solution will not be applicable for a system containing two magnets as they would never leave the dipped section of the arc where they are closest together in distance. In order to translate this problem to that faced by two magnets in the system presented here, it is necessary for the field to be dependent on the distance between the current point on the curve and the ground.

Gomez et al.[89] derive a generalised solution to the Brachistochrone problem that can take equations for the gravitational field of the form $(Ay + B)^n$:

$$x = \int \sqrt{\frac{2T^2}{m\pi^2} n^2 A^2 (Ay + B)^{n-2} - 1} dy \tag{8.3}$$

where m is the mass of the particle travelling down the path and T is the time when the particle reaches the end of the curve. If $A = 0$, $B = mg$ and $n = 1$ then the equation outputs the typical solution to the Brachistochrone Problem. For the system here, the formula of the gravitional potential field requires $A = 1$, $B = 0$ and $n = -3$. After substituting these values, the equation simplifies to

$$x = \frac{T\sqrt{6}}{\pi} \int \sqrt{-y^{-5} - K} dy \tag{8.4}$$

where $K = \frac{\pi}{T\sqrt{6}}$. This could then be solved to find a path which would allow the magnets to reach their final positions as quickly as possible. However, the solution is still dependent on s being equal to zero.

Finally, it should be noted that these candidate methods of optimization both ignore the fact that, while two magnets in a curved path are approaching each other, they are simultaneously moving further away from the magnets in their own tiles. It is here that the solution begins to resemble the classical n-body problem and optimizations become significantly more difficult to attain. For example, even if the optimal solution (with regards to an as-yet undecided criteria) is found for a system of three tiles comprising

one linear propagation followed by one 90° turn, will it still be optimal for a system of three tiles comprising one 90° turn followed by one linear propagation? If this isn't the case, how many path types would be necessary in order to produce an optimal solution in every possible configuration of tiles? Would infinitely many be necessary? Questions of this type are still open for investigation.

Although the system works successfully in terms of simulated and experimental results, it is not proven to be definitively optimal and a definitive method for optimisation has not decided upon. It is predicted that further optimisation will be necessary in order for systems comprising smaller tiles to function. This will most likely require numerical solutions of large systems of functions relating the positions and forces acting upon each magnet in a given system at each time step.

8.2.3 Further Functionality

This work has focused on the concept of a chain folding into a shape; in other words, a $1D \rightarrow 2D$ system. An ideal system would be able to self-assemble from individual modules to a three-dimensional shape: a $0D \rightarrow 1D \rightarrow 2D \rightarrow 3D$ system. In order to allow the two-dimensional shape to fold into three dimensions, the current method of using circles to illustrate the relative distances between magnets could be replaced by spheres and the inequalities presented here could be augmented to include distances in the z-axis. An environment that would allow the chain to assemble in three dimensions uninhibited would also need to be established. The planning of how the structure should be built such that it doesn't self-intersect will be a required subject for further research.

Attaining the first part of the ideal system, that of parts assembling into a chain, is presumed to be more simple than allowing the creation of a three-dimensional structure. As mentioned in the previous chapter, the tiles are roughly attracted to each other in a chain-like manner due to the magnet locations in each tile. Further development of the hinge design would need to be carried out to ensure that the tile hinges always align correctly, most likely in a similar fashion to the technique used by Virgo et al[2].

Another possibility for future development would be the ability to create more complex configurations. For example, the angle of folding between each pair of tiles could be varied simply by varying the angles of the external tile walls. Alternatively, making the tile shape circular and varying the final magnet positions in curved paths would also produce the same result but while maintaining the property that all of the tiles' external geometries are identical. Both of these modifications would allow the opportunity for more complex structures to be produced. Thinking further ahead, by incorporating more magnets in the tiles such that propagation can be initiated/inhibited, it may be possible

to demonstrate logic such as AND, OR etc. based on the output when the chain has finished being actuated. This would demonstrate the ability for the system to perform computation.

Appendix A

Design iterations for folding paths

FIGURE A.1: Miyashita-type design where paths for folding are asymmetric. The distance between magnets in paths decreases monotonically but there is difficulty during experiments in moving a magnet along the path that is not angled.

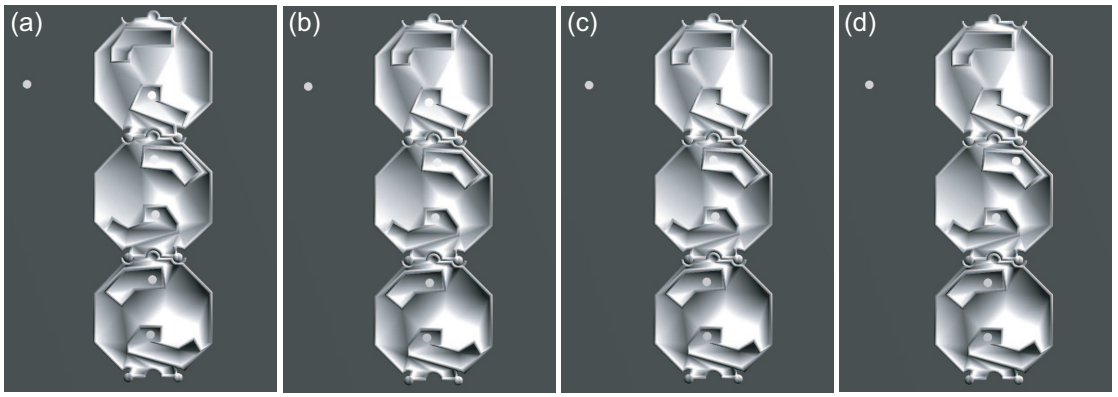

FIGURE A.2: Miyashita-type design produced by the author. (a) M1 is initiated by the RI. (b) M1 is pulled around the path by the RI and initiates movement of M2. (c) M1 and M2 travel along their respective paths. (d) M1 and M2 do not initiate a folding motion and M3 travels a short distance along its path, but M3 cannot travel far enough for propagation to occur.

Appendix B

The Blender Simulation Environment

Blender is a 'free and open-source 3D creation suite'[90] created in 1995. It can be used for rendering, 3D modelling, animation, and simulations amongst many other applications. It was decided (in collaboration with Valentin Besnard) that Blender was a suitable program for developing simulations in this project for two main reasons: It can simulate collisions between convex meshes with a high level of accuracy due to its usage of the Bullet physics library[91], and the visual output is of a very high quality in comparison to other 3D graphics software such as OpenGL.

B.1 Magnet and Tile Simulations

The simulations for this system were created entirely in the Blender Game Engine Version 2.78a. Tile models designed using Autodesk Fusion 360 were imported as COLLADA files and modelled as static objects. This caused the tiles to be considered as 'massless' and any tile motion is entirely dependent on the Python scripts linked to them instead of motion caused by the physics engine. Magnets were designed as cylindrical meshes of dynamic type in order for the physics engine to be applied to them. Magnets were given mass, but not friction. Damping was also included. A Python script separate to that of the tiles was linked to each magnet.

B.2 Python Scripts

Both Python scripts were initially created by Valentin Besnard. Improvements were made by the author to both increase accuracy of magnet movement and increase simulation speed and efficiency. The magnet script calculates the force acting upon a magnet by the adjacent magnets in the chain. If magnets are in their initial positions and no magnet has come close enough to initiate movement, then its dynamics are suspended to reduce computation and prevent magnets from automatically being actuated. Meanwhile, the tile script determines when folding of the chain should begin and when collisions between tiles have occurred. If the tiles are not required to move then they are put into 'sleep mode'. Although significant improvements in performance were realised, it would be incorrect to assume that either script is optimal and it is likely that systems containing more than 1000 tiles will be slow if further optimisations are not carried out. The figures below are screen shots showing details of the simulation setup and features. Videos of the simulations are available online.

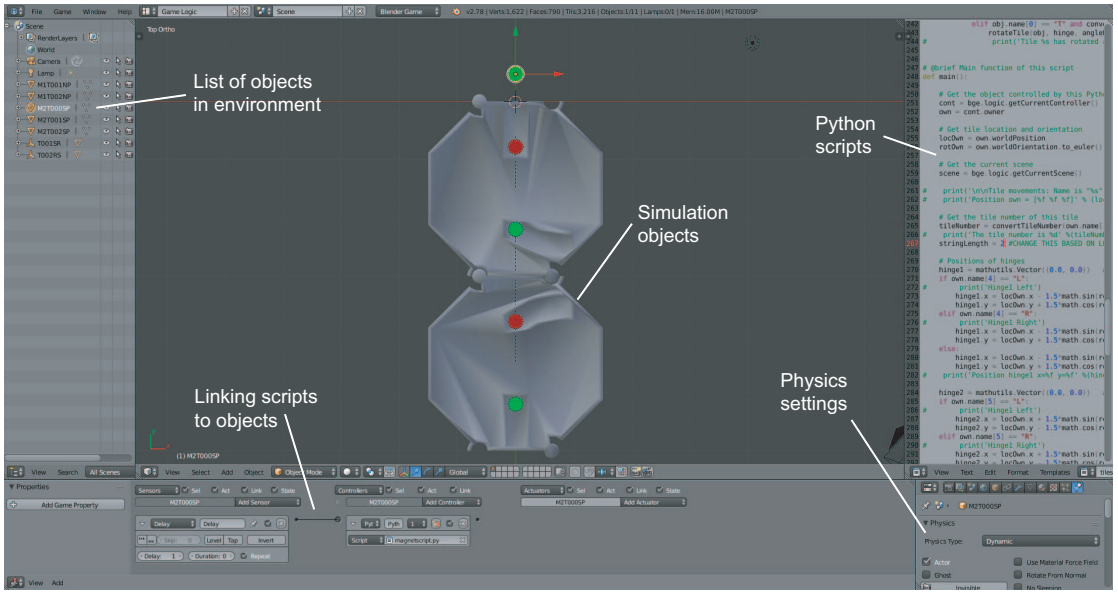

FIGURE B.1: Blender environment in the set-up used for developing the simulations in this work.

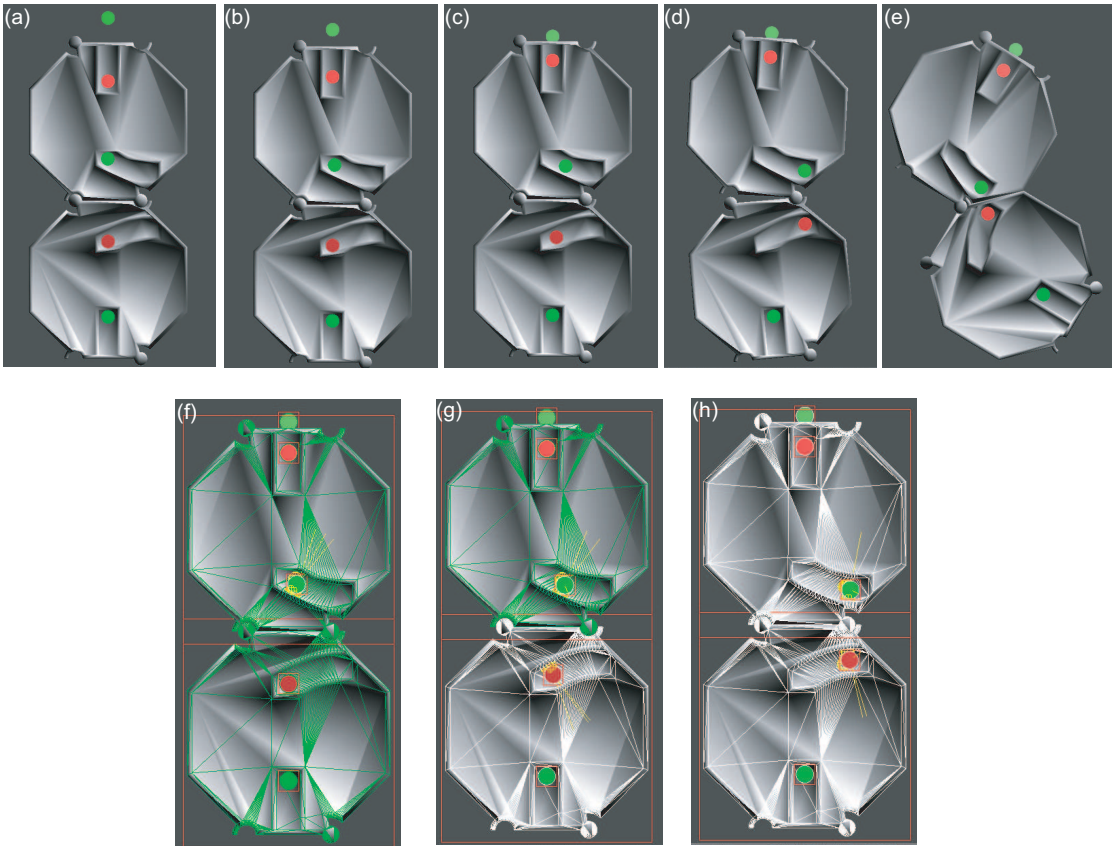

FIGURE B.2: Examples of the simulation environment being used. (a)-(e) Stages of propagation during a Blender simulation. (f)-(h) Visualisation of simulation physics indicates the logic used to improve quality. Active magnets are surrounded in yellow lines, absence of yellow lines indicate that the magnet dynamics are suspended until activated by another magnet. Tiles in 'sleep mode' are outlined in green, while tiles that have not yet begun to move are outlined in white.

Bibliography

[1] Lionel Penrose. Self-reproducing machines. *Scientific American*, 200:105–114, June 1959.

[2] Nathaniel Virgo, Chrisantha Fernando, Bill Bigge, and Phil Husbands. Evolvable physical self-replicators. *Artificial Life*, 18(2):129–142, April 2012.

[3] Mustafa Emre Karagozler, Seth Copen Goldstein, and James Robert Reid. Stress-driven MEMS assembly + electrostatic forces = 1mm diameter robot. In *Proceedings of the IEEE International Conference on Intelligent Robots and Systems (IROS '09)*, pages 2763–2769, Oct 2009.

[4] Mila Boncheva and George M. Whitesides. Making things by self-assembly. *MRS Bulletin (Self-Assembly in Materials Synthesis)*, 30(10):736–742, October 2005.

[5] Yiqi Mao, Kai Yu, Michael S. Isakov, Jiangtao Wu, Martin L. Dunn, and H. Jerry Qi. Sequential self-folding structures by 3d printed digital shape memory polymers. *Nature Scientific Reports*, 5:1–12, September 2015.

[6] Sehyuk Yim and Metin Sitti. SoftCubes: Stretchable and self-assembling three-dimensional soft modular matter. *The International Journal of Robotics Research*, 33(8):1083–1097, 2014.

[7] Sehyuk Yim and Metin Sitti. SoftCubes: Towards a soft modular matter. In *Proceedings of the IEEE International Conference on Robotics and Automation (ICRA)*, pages 530–536. IEEE, 2013.

[8] Jurg Germann, Andrea Maesani, Ramon Pericet-Camara, and Dario Floreano. Soft cells for programmable self-assembly of robotic modules. *Soft Robotics*, 1(4):239–245, 2014.

[9] Paul W. K. Rothemund. Folding DNA to create nanoscale shapes and patterns. *Nature*, 440:297–302, 2006.

[10] Johndale C.Solem. Self-assembling micrites based on the platonic solids. *Robotics and Autonomous Systems*, 38:69–92, February 2002.

[11] Amit Kessel and Nir Ben-Tal. *Introduction to Proteins: Structure, Function, and Motion*, volume 1 of *1*. CRC Press, Boca Raton, U.S.A, 1 edition, 2 2001.

[12] Joseph D. Bryngelson, Jos Nelson Onuchic, Nicholas D. Socci, and Peter G. Wolynes. Funnels, pathways, and the energy landscape of protein folding: A synthesis. *Proteins: Structure, Function, and Bioinformatics*, 21:167–195, March 1995.

[13] Hue Sun Chan and Ken A. Dill. Protein folding in the landscape perspective: Chevron plots and non-arrhenius kinetics. *Discrete and Computational Geometry*, 30:2–33, January 1998.

[14] Shuhei Miyashita, Christof Audretsch, Zoltn Nagy, Rudolf N. Fchslin, and Rolf Pfeifer. Mechanical catalysis on the centimeter scale. *Journal of the Royal Society Interface*, 12(4), 2015.

[15] Kenneth C. Cheung, Erik D. Demaine, Jonathan R. Bachrach, and Saul Griffith. Programmable assembly with universally foldable strings (Moteins). *IEEE Transactions on Robotics*, 27(4):718–729, 2011.

[16] Esther M Arkin, P Fekete, and Joseph S.B Mitchell. An algorithmic study of manufacturing paperclips and other folded structures. *Computational Geometry*, 25:117–138, May 2003.

[17] Alexander I. Oparin. The origin of life. *Moscow Worker Publisher*, 1924 (in Russian).

[18] Vuk Uskokovic. Isn't self-assembly a misnomer? Multi-disciplinary arguments in favor of co-assembly. *Advances in Colloid and Interface Science*, 141:37–47, September 2008.

[19] Julianne D. Halley and David A. Winkler. Consistent concepts of self-organsization and self-assembly. *Complexity*, 14:10–17, July 2008.

[20] George M. Whitesides and Bartosz Grzybowski. Self-assembly at all scales. *Science*, 295(5564):2418–2421, 2002.

[21] Paul William Anderson. More is different. *Science*, 177:393–396, August 1972.

[22] Mark A. Bedau. Weak emergence. *Nous*, 31:375–399, 1997.

[23] Vincent C. Mller and Matej Hoffmann. What is morphological computation? on how the body contributes to cognition and control. *Artificial Life*, 23:1–24, February 2017.

[24] William M. Jacobs and Daan Frenkel. Self-assembly of structures with addressable complexity. *Journal of the American Chemical Society*, 138:2457–2467, March 2016.

[25] Atsushi Masumori and Hiroya Tanaka. Morphological computation on two dimensional self-assembly system. In *ACM SIGGRAPH 2013 Posters, SIGGRAPH 2013*, 2013.

[26] Mila Boncheva, David H. Gracias, Heiko O. Jacobs, and George M. Whitesides. Biomimetic self-assembly of a functional asymmetrical electronic device. *Proceedings of the National Academy of Sciences*, 99:4937–4940, April 2002.

[27] Mitsuharu Matsumoto and Shuji Hashimoto. Passive self-replication of millimeter-scale parts. *IEEE Transactions on Automation Science and Engineering*, 6(2):385–391, 2009.

[28] Masayoshi Mitsui, Atsushi Masumori, Ryo Asakura, and Hiroya Tanaka. Applying self-assembly and self-reconfigurable sytems for printer. In *ALIFE 14*, pages 539–540. MIT Press, 2014.

[29] Andrea Vergara, Yi sheng Lau, Ricardo-Franco Mendoza-Garcia, and Juan Cristbal Zagal. Soft modular robotic cubes: Toward replicating morphogenetic movements of the embryo. *PLOS ONE*, 12, January 2017.

[30] Jungwon Seo, Mark Yim, and Vijay Kumar. Assembly sequence planning for constructing planar structures with rectangular modules. In *Proceedings of the IEEE International Conference on Robotics and Automation (ICRA)*, pages 5477–5482. IEEE, 2016.

[31] Irene Parada, Vera Sacristan, and Rodrigo I. Silveira. A new meta-module for efficient reconfiguration of hinged-units modular robots. In *Proceedings of the IEEE International Conference on Robotics and Automation (ICRA)*, pages 5197–5202. IEEE, 2016.

[32] Ayan Dutta and Prithviraj Dasgupta. Simultaneous configuration formation and information collection by modular robotic systems. In *Proceedings of the IEEE International Conference on Robotics and Automation (ICRA)*, pages 5197–5202. IEEE, 2016.

[33] Hiroshi Kawano. Full-resolution reconfiguration planning for heterogeneous cube-shaped modular robots with only sliding motion primitive. In *Proceedings of the IEEE International Conference on Robotics and Automation (ICRA)*, pages 5222–5229. IEEE, 2016.

[34] M. Yim, P. White, M. Park, , and J. Sastra. Modular self-reconfigurable robots. In Robert A. Meyers and Warren Dixon, editors, *Encyclopedia of Complexity and Systems Science*, chapter 2, pages 19–32. Springer, 2009.

[35] Haruhisa Kurokawa, Kohji Tomita, Akiya Kamimura, Shigeru Kokaji, Takashi Hasuo, and Satoshi Murata. Distributed self-reconfiguration of M-TRAN III modular robotic system. *International Journal of RObotics Research*, 27:7373–386, March/April 2008.

[36] Satoshi Murata, Kiyoharu Kakomura, and Haruhisa Kurokawa. Toward a scalable modular robotic system. *IEEE Robotics and Automation Magazine*, 14:56–63, December 2007.

[37] Seth Copen Goldstein and Peter Lee. Realizing programmable matter, 2006. [Online; accessed 21-August-2017].

[38] Mitchell R. Zakin. Defense sciences research and technology special focus area: Programmable matter, 2007. [Online; accessed 21-August-2017].

[39] Kyle Gilpin, Ara Knaian, and Daniela Rus. Robot pebbles: One centimeter modules for programmable matter through self-disassembly. In *2010 IEEE International Conference on Robotics and Automation (ICRA)*, pages 2485–2492, May 2010.

[40] Kazuhiro Saitou. Conformational switching in self-assembling mechanical systems. *IEEE Transactions on Robotics and Automation*, 15:510–520, June 1999.

[41] Chengde Mao, Venkat R. Thalladi, Daniel B. Wolfe, Sue Whitesides, and George M. Whitesides. Dissections: Self-assembled aggregates that spontaneously reconfigure their structures when their environment changes. *JACS Communications*, 124(49):14508–14509, 2002.

[42] Ned Bowden, Scott R. J. Oliver, and George M. Whitesides. Mesoscale self-assembly: Capillary bonds and negative menisci. *Journal of Physical Chemistry*, 104:2714–2724, 2000.

[43] Ned Bowden, Andreas Terfort, Jeff Carbeck, and George M. Whitesides. Self-assembly of mesoscale objects into ordered two-dimensional arrays. *Science*, 276(5310):233–235, 1997.

[44] Hiroaki Onoe, Kiyoshi Matsumoto, and Isao Shimoyama. Three-dimensional sequential self-assembly of microscale objects. *Small*, 3:1383–1389, June 2007.

[45] Kazuo Hosokawa, Isao Shimoyama, and Hirohumi Miura. Dynamics of self-assembling systems: Analogy with chemical kinetics. *Artificial Life*, 1:413–427, 1994.

[46] Patrick Ryan and Eric Diller. Five-degree-of-freedom magnetic control of micro-robots using rotating permanent magnets. In *Proceedings of the IEEE International Conference on Robotics and Automation (ICRA)*, pages 1731–1736. IEEE, 2016.

[47] Mohammad Salehizadeh and Eric Diller. Two-agent formation control of magnetic microrobots in two dimensions. *Journal of Micro-Bio Robotics*, 12:9–19, June 2017.

[48] U Kei Cheang, Farshad Meshkati, Hoyeon Kim, Kyoungwoo Lee, Henry Chien Fu, and Min Jun Kim. Versatile microrobotics using simple modular subunits. *Nature Scientific Reports*, 6:1–10, 2016.

[49] U Kei Cheang, Kyoungwoo Lee2, Anak Agung Julius, , and Min Jun Kim. Multiple-robot drug delivery strategy through coordinated teams of microswimmers. *Applied Physics Letters*, 105:1–5, August 2014.

[50] Wendong Wang, Joshua Giltinan, Svetlana Zakharchenko1, and Metin Sitti. Dynamic and programmable self-assembly of micro-rafts at the air-water interface. *Science Advances*, 3, May 2017.

[51] Eiji Iwase and Isao Shimoyama. A design method for out-of-plane structures by multi-step magnetic self-assembly. *Sensors and Actuators A: Physical*, 127:310–315, September 2006.

[52] Xiaotian Ma, Dana Vogtmann, and Sarah Bergbreiter. Dynamics and scaling of magnetically folding multi-material structures. In *Robotics and Automation (ICRA), 2016 IEEE International Conference on*, pages 1899–1906, 2016.

[53] Sheetal B. Shetye, Ilan Eskinazi, and David P. Arnold. Self-assembly of millimeter-scale components using integrated micromagnets. *IEEE Transactions on Magnetics*, 44(11):4293–4296, 2008.

[54] Atsushi Masumori, Masayoshi Mitsui, and Hiroya Tanaka. Designing a passive folding string device with an electromagnet. In *Proceedings of the Fourteenth International Conference on the Synthesis and Simulation of Living Systems*, number 14 in ALIFE '14, pages 987–988, 2014.

[55] Hanying Lib, Joshua D.Cartera, and Thomas H.LaBean. Nanofabrication by DNA self-assembly. *Materials Today*, 12:24–32, May 2009.

[56] M.B. Cohn, C.J. Kim, and A.P. Pisano. Self-assembling electrical networks: an application of micromachining technology. In *Proceedings of the 1991 International Conference on Solid-State Sensors and Actuators (TRANSDUCERS '91)*, pages 490–493. IEEE, 1991.

[57] Bruce Hajek. Cooling schedules for optimal annealing. *Mathematics of Operations Research*, 13:311–329, May 1988.

[58] Karl-Friedrich Bohringer, Ken Goldberg, Michael Cohn, Roger Howe, and Al Pisano. Parallel microassembly with electrostatic force fields. In *Robotics and Automation, 1998. Proceedings. 1998 IEEE International Conference on*, pages 1204–1211. IEEE, 1998.

[59] Shuhei Miyashita, Zoltn Nagy, Bradley J. Nelson, and Rolf Pfeifer. The influence of shape on parallel self-assembly. *Entropy*, 11(4):643–666, 2009.

[60] Michael T. Tolley, Mekala Krishnan, David Erickson, and Hod Lipson. Dynamically programmable fluidic assembly. *Applied Physics Letters*, 93:93–95, December 2008.

[61] Pablo F. Damasceno, Michael Engel, and Sharon C. Glotzer. Predictive self-assembly of polyhedra into complex structures. *Science*, 337:453–457, July 2012.

[62] Elizabeth R. Chen, Daphne Klotsa, Michael Engel, Pablo F. Damasceno, and Sharon C. Glotzer. Complexity in surfaces of densest packings for families of polyhedra. *Physical Review X*, 4:1–23, February 2014.

[63] Greg van Anders, N. Khalid Ahmed, Ross Smith, Michael Engel, and Sharon C. Glotzer. Entropically patchy particles: Engineering valence through shape entropy. *ACS Nano*, 8:931–940, December 2014.

[64] Jatinder S. Randhawa, Levi N. Kanu, Gursimranbir Singh, and David H. Gracias. Importance of surface patterns for defect mitigation in three-dimensional self-assembly. *Langmuir*, 26(15):12534–12539, 2010.

[65] MIT Center for Bits and Atoms. (Tiny) reconfigurable robots at MIT, 2012. [Online; accessed 3-August-2017].

[66] Matthew D. Hancher and Gregory S. Hornby. A modular robotic system with applications to space exploration. In *Proceedings of the Second IEEE International Conference on Space Mission Challenges for Information Technology*, pages 124–132. IEEE, 2006.

[67] Christian B. Anfinsen. Principles that govern the folding of protein chains. *Science*, 181:223–230, July 1973.

[68] Franz-Ulrich Hartl. Molecular chaperones in cellular protein folding. *Nature*, 381:571–580, June 1996.

[69] Cyrus Levinthal. How to fold graciously. In *Mossbauer Spectroscopy in Biological Systems Proceedings*, pages 22–24. University of Illinois Bulletin, 1969.

[70] Ron Unger and John Moult. Finding the lowest free energy conformation of a protein is an NP-hard problem: proof and implications. *Bulletin of Mathematical Biology*, 55:1183–1198, January 1993.

[71] Marcos N. Betancourt and D. Thirumalai. Protein sequence design by energy landscaping. *Journal of Physical Chemistry B*, 106:599–609, December 2002.

[72] P. E. Leopold, M. Montal, and J. N. Onuchic. Protein folding funnels: a kinetic approach to the sequence-structure relationship. *Proceedings of the National Academy of Sciences*, 89:8721–8725, September 1992.

[73] Valentin Besnard. Simulation, analysis and design of self-assembly microrobots, August 2016. Internal document at the University of York.

[74] Alon Itai, Christos H. Papadimitriou, and Jayme Luiz Szwarcfiter. Hamilton paths in grid graphs. *SIAM Journal on Computing*, 11:676–686, November 1982.

[75] Erik Demaine. *Folding and Unfolding.* PhD thesis, University of Waterloo, Waterloo, ON, 2001.

[76] Robert Connelly, Erik D. Demaine, and Gunter Rote. Straightening polygonal arcs and convexifying polygonal cycles. In *Proceedings of the 41st Annual Symposium on Foundations of Computer Science*, pages 1–49. IEEE, 2000.

[77] Ileana Streinu. A combinatorial approach to planar non-colliding robot arm motion planning. In *Proceedings of the 41st Annual Symposium on Foundations of Computer Science*, pages 1–9. IEEE, 2000.

[78] Gino van den Bergen. A fast and robust GJK implementation for collision detection of convex objects. *Journal of Graphics Tools*, 4:7–25, July 1999.

[79] Charbel Fares and Ar Hamam. Collision detection for rigid bodies: A state of the art review. In *In GraphiCon*, 2005.

[80] Pankaj K. Agarwal, Julien Basch, Leonidas J. Guibas, John Hershberger, and Li Zhang. Deformable free-space tilings for kinetic collision detection. *The International Journal of Robotics Research*, 21:179–197, March 2002.

[81] L.J.de Vin, J.de Vries, A.H.Streppel, E.J.W.Klaassen, and H.J.J.Kals. The generation of bending sequences in a CAPP system for sheet-metal components. *Journal of Materials Processing Technology*, 41:331–339, March 1994.

[82] Mark de Berg, Otfried Cheong, Marc van Kreveld, and Mark Overmars. *Computational Geoemety: Algorithms and Applications.* Springer, 2008.

[83] Autodesk Fusion 360. Home — Autodesk Fusion 360, 2017. [Online; accessed 1-August-2017].

[84] Supermagnete. Home — supermagnete, 2017. [Online; accessed 1-August-2017].

[85] Timothy G. Leong, Aasiyeh M. Zarafshar, and David H. Gracias. Three-dimensional fabrication at small size scales. *Small*, 6:792–806, March 2010.

[86] Snaak LLC. Snaak: Millions of shapes in your hands, 2014. [Online; accessed 16-August-2017].

[87] Fabian D. Natterer, Kai Yang, William Paul, Philip Willke, Taeyoung Choi, Thomas Greber, Andreas J. Heinrich, and Christopher P. Lutz. Reading and writing single-atom magnets. *Nature*, 543:226–228, March 2017.

[88] Ronald S. Fearing. Survey of sticking effects for micro parts handling. In *Proceedings of the IEEE/RSJ International Conference on Intelligent Robots and Systems*, pages 212–217. IEEE, 1995.

[89] R. Gomez, V. Marquina, and S. GomezAiza. An alternative solution to the general tautochrone problem. *Revista Mexicana de Fisica E*, 54:212–215, December 2008.

[90] Blender. Home — Blender, the free and open-source 3D creation suite, 2017. [Online; accessed 1-August-2017].

[91] Bullet Physics Library. Home — Bullet physics library, 2017. [Online; accessed 1-August-2017].